CEMENTEGRITY CEMENTEGRITY – ACT Project no. 327311

Characterisation and monitoring of oil-well cements under simulated CCS well conditions

Report for WP5 of the CEMENTEGRITY Project

UK ACT ERA-NET EC PROJECT NUMBER 691712

Department for Energy Security and Net Zero (2025)

Acknowledgements

This project was funded through the Accelerating Carbon Capture and Storage Technologies (ACT) 3, part of Horizon 2020 (UK Project No 691712). Funding from the Research Council of Norway, the Netherlands Enterprise Agency, the UK Department for Energy Security and Net Zero, and Harbour Energy is gratefully acknowledged. The authors also wish to acknowledge the support of the other consortium members: Institute for Energy Technology, Halliburton AS, ReStone AS, University of Stavanger, Delft University of Technology, Energie Beheer Nederland, and Harbour Energy.

Contents

Executive Summary

ACT 3 was an international collaboration involving 14 countries, including the UK, to advance CCUS technologies through funding for research and innovation. The UK's involvement, supported by the BEIS Net Zero Innovation Portfolio, offered up to £5 million in grants until March 2025 to assist CCUS developers in increasing technology readiness levels. This funding contributed to a £40 million pool, with £25 million provided by ACT partners. Established in 2015, ACT promotes international cooperation, with consortia led by one country and involving at least two others. ACT 3 built on the successes of ACT 1 and 2, which supported 15 UK projects, facilitating international partnerships, knowledge sharing, and advancing CCS technologies towards commercial use.

Under the ACT 3 programme, Heriot-Watt University participated in the Development and Testing of Novel Cement Designs for Enhanced CCS Well Integrity (CEMENTEGRITY) project, which aimed to investigate mechanisms of potential leakage within or around wellbore seals in CCS reservoirs. The primary objective of the project was to identify key properties of representative cementitious sealants for maintaining long-term seal integrity. Five sealant compositions, based on three binder technologies with varying TRLs, were studied, focusing on three main capabilities: (i) forming and maintaining a seal, (ii) resisting exposure to CO2-bearing fluids, and (iii) withstanding thermal shocks or cycling. Overall, the findings indicated that while none of the representative sealant blends demonstrated superior performance across all aspects, optimal performance could potentially be achieved by tailoring specific sealant blends for different parts of the wellbore system, adapted to local conditions. The outcomes also highlight opportunities for developing more versatile and adaptable blends.

This report focuses on the first capability, investigated through Work Package (WP) 5 at Heriot-Watt University, which employed shear-bond testing. WP5 also evaluated the potential of electrical measurements to characterise and monitor the bulk properties of the sealants and of the sealant/steel interface. Key findings from this WP include:

(1) Mean apparent bond strength was influenced by various factors, including curing conditions, sealant setting time, and corrosion at the interface between sealant and steel casing. Bond strength was found to be related to compressive strength, but high compressive strength did not necessarily guarantee good bonding performance.

(2) Elevated curing temperatures and pressures significantly improved both shear-bond and compressive strengths. The elevated curing pressure proved particularly effective in reducing volumetric changes during the extended curing, hence improving apparent mean bond strength measured.

(3) Electrical measurements demonstrated promise for monitoring hydration processes and assessing sealant permeability. Using the steel casing as one of the electrodes, variations in response were observed, which were attributed to corrosion initiation at the sealant/steel casing interface. This demonstrates the potential of these methods to monitor the sealant and the condition at the interface.

1.0 Introduction

The CEMENTEGRITY consortium was established in 2021 with the purpose of advancing research into the development and assessment of representative materials for sealing wellbores exposed to CO_2 stored within underground reservoirs. This project was undertaken from October 2021 to December 2023 and received funding through the ACT programme Phase 3 (Accelerating CCS Technologies, Horizon2020 Project No 691712), which supports innovation in CCS technologies. Financial contributions were provided by the Research Council of Norway (RCN), the Netherlands Enterprise Agency (RVO), the Department for Energy Security & Net Zero (DESNZ, UK), and Harbour Energy.

The consortium brought together a wealth of expertise from leading institutions and companies based in Norway, the Netherlands, and the United Kingdom. These included the Institute for Energy Technology, Halliburton AS, ReStone AS, Universitetet I Stavanger, Delft University of Technology, EBN BV, Heriot-Watt University, and Harbour Energy.

For further information about the project, readers are invited to visit the CEMENTEGRITY website at https://www.cementegrity.eu

2.0 Project Outline

The aim of the CEMENTEGRITY project was to investigate the mechanisms of potential leakage within or around wellbore seals within CCS reservoirs. The primary objective was to identify key properties of cementitious sealants that ensure long-term seal integrity. This objective was addressed through seven integrated work packages (WPs), summarised as follows:

WP1: Effects of dissolved and supercritical CO_2
WP2: Impact of CO_2 with impurities on the integrity of wellbore sealants in CCS
WP3: Thermomechanical behaviour of wellbore sealants
WP4: Numerical simulation of reaction and microstructure development of novel sealant
WP5: Interfacial and bulk properties of cement sealants
WP6: Development of rock-based geopolymers for CCS applications
WP7: Identification of critical properties and suitable testing methods for sealants in CCS applications

Five sealant compositions, based on three binder technologies with varying Technology Readiness Levels (TRLs), were studied across the participating institutions. The work focused on three key performance abilities:
(i) forming and maintaining a seal,
(ii) resisting exposure to CO_2-bearing fluids, and
(iii) withstanding thermal shocks or cycles.

This report presents a summary of the activities carried out as part of WP 5 at Heriot-Watt University, addressing the first key performance capability. The work focused on two primary areas: (i) the assessment of the bonding performance of sealants to metal casing, and (ii) the characterisation and monitoring of the bulk properties of the sealants studied within the project, along with the sealant/steel interface. A summary of the key findings from the activities undertaken in the CEMENTEGRITY project can be found in the ACT-CEMENTEGRITY Final Report available at https://www.act-ccs.eu/archive

3. Role and Contributions of Each Project Partners

A detailed description of the roles and contributions of the project partners can be found in the ACT-CEMENTEGRITY Final Report. Below is a summary:

The Institute for Energy Technology (IFE) led the CEMENTEGRITY consortium, with Dr Reinier van Noort serving as the Project Coordinator, National Coordinator for Norway, and leader of Work Package 7 (WP7). Supporting this effort was Dr Gaute Svenningsen, who led WP2. Halliburton AS made significant contributions through Gunnar Lende, who served as the leader of WP1 and supported the fabrication and distribution of all test samples required for testing in all WPs, ensuring consistent preparation and curing. ReStone AS added technical expertise, with Dr Astri Kvassnes collaborating on WP1 and WP5, as well as providing technical advice to the consortium. At the Universitetet i Stavanger, Prof Mahmoud Khalifeh led WP6, supported by a PhD student Seyed Hasan Hajiabadi.

Delft University of Technology brought expertise through Dr Anne Pluymakers, who acted as the National Coordinator for the Netherlands and leader of WP3, supported by Dr Kai Li. In addition, Prof Guang Ye led WP4 and assisted by Dr Xiujiao Qiu and Dr Mayank Gupta in developing a numerical model for the rock-based geopolymer sealant designed by Universitetet i Stavanger. EBN BV offered an industry perspective, through Marco op de Weegh and Klaas Hartsema providing technical inputs.

Heriot-Watt University (HWU) was represented by Dr Benny Suryanto, who acted as the National Coordinator for the UK and led WP5, supported by Dr Gerard Starrs. Lastly, Harbour Energy played an integral role as both a funder and technical advisor, with Oliver Czuprat contributing important insights from an industry perspective.

4. Description of WP5

The key outcomes from each work package in the CEMENTEGRITY project are detailed in the ACT-CEMENTEGRITY Final Report. This section offers an overview of the methodology and key findings of Work Package (WP) 5, with a particular emphasis on the characterisation and monitoring of the interfacial and bulk properties of cement sealants.

4.1 Background

In light of the projected timescales envisaged for the operation of CCS storage facilities, which is well in excess of the lifespan of traditional oil and gas wells, minimising the leakage of CO2 is of utmost importance for effective CCS storage performance. **Figure 1** shows a schematic representation of the structure of a plugged wellbore, illustrating the natural rock formation and the steel casing of the wellhead, with the potential pathways for leakage of CO2 highlighted. These pathways include leakage through the external casing/well-head interface, the internal casing/well-head interface, the wellhead microstructure and/or internal fractures, as well as the external cement sheath/rock interface.

Figure 1. Schematic representation of possible leakage pathways in a CCS well

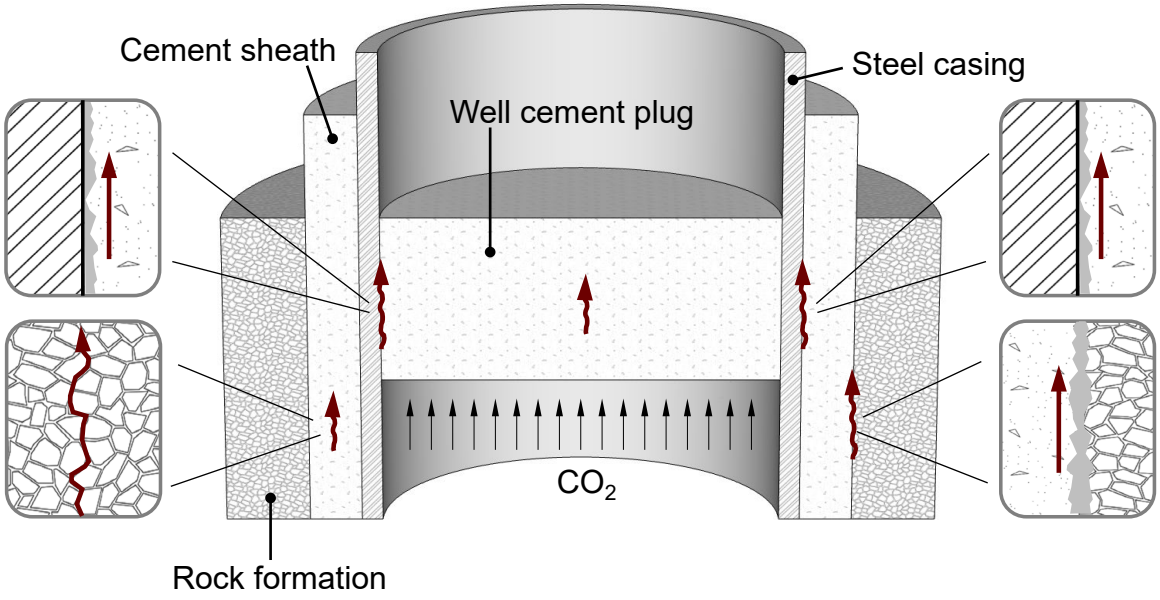

To minimise the risk of CO2 leakage, whether in its liquid, dissolved, or gaseous form, it is essential to ensure good adhesion between the well-plug, the surrounding rock formation, and the wellbore casing. Historically, the adhesion of well-plug sealant materials to the surrounding casing or rock formation has been assessed using a variety of bond tests (e.g., shear bond test, hydraulic bond test, gas bond test, or a combination thereof). Shear bond measures the shear strength of an interface and is generally obtained by measuring the force required to initiate movement of a cement plug encased in a metal cylinder, or a pipe or rod embedded in a cement cylinder. Hydraulic bond evaluates the resistance between cement and surrounding

casing and/or formation to fluid migration and is typically assessed by measurement of the flow of hydraulic fluid through an interface over time. The principle of gas bond is similar in many respects to hydraulic bond but relies on the measurement of gas migration instead of fluid migration. Due to the nature of the tests, hydraulic and gas bond can be expected offer a more direct representation of interface leakage performance. However, the tests are generally much more difficult to perform and more sensitive to experimental errors caused by gas leakage from the pressure containment cell and ballooning effects.

WP 5 focuses on the characterisation of the interfacial and bulk properties of selected representative sealants. To this end, we have developed laboratory-based test procedures designed to assess the shear bond strength of cementitious sealants encased within rigid (in this case, metal) cylinders. The following sections detail the test methodology, focusing on test procedures that can be easily implemented within standard cement and concrete testing laboratory facilities. This report also outlines how this test methodology is applied to evaluate the bond performance of CEMENTEGRITY sealants. The majority of the test samples were subjected to an enhanced curing regime, intended to achieve thorough hydration within the timeframe of the project and replicate certain aspects of the high-temperature and high-pressure conditions typical of a subsea wellbore. Non-destructive testing methods, employing electrical property measurements, were also conducted in parallel with the shear-bond tests, both during and after the enhanced curing process, to provide insights into the bulk properties of the sealants and information for future classification and performance evaluation. The findings from this WP complement the results obtained using various investigative techniques across other WPs. This report provides a summary of the methodology and key outcomes of WP 5.

4.2 Experimental Programme

4.2.1 Materials

The sealants utilised in this WP are summarised in **Table 1**, alongside their specific gravity and Technology Readiness Level (TRL). Sealant S1 represents a material commonly used in older oil and gas wells, comprising standard Portland cement Class G combined with silica flour (35% by weight).

The remaining sealants are proprietary products, and their full details cannot be disclosed. Sealant S2 also serves as a wellbore plugging material, incorporating an expansive agent and mineral additive designed to achieve exceptionally low permeability. Sealant S3 is an enhanced version of Sealant S2, enriched with CO2-sequestering mineral additives, including RePlug®. Sealant S4, a proprietary calcium aluminate blend, is currently employed in high-temperature wells and is noted for its excellent resistance to acid. Sealant S5 is a geopolymer sealant formulated from a mixture of precursors, with granite included as a filler material. Sealants S3, S4, and S5 have been identified as proprietary formulations specifically for use in new CCS wells. **Table 2** provides the typical oxide composition of Portland cement.

Table 1: Summary of sealant materials

ID	Description	SG	TRL
S1	Standard Portland cement (PC)-silica blend	1.9	7
S2	Reduced permeability PC-silica blend for field use	1.9	7
S3	PC-silica blend with reduced permeability, containing CO2 sequestering mineral additive RePlug®	1.9	3
S4	Calcium aluminate cement-based blend	1.8	7
S5	Geopolymer using granite as one of the precursors	1.9	3

Table 2: Oxide analysis of Portland cement

CaO	SiO_2	Al_2O_3	Fe_2O_3	MgO	MnO	TiO_2	Sr	SO_3	K_2O	Na_2O
62	19.6	4.08	5.94	1.19	0.12	0.25	0.2	4.1	0.8	0.17

The bond test sample was designed as a scaled-down representation of a plugged wellbore, consisting of an outer cylindrical steel casing and an internal cement plug, as illustrated in **Figure 2**. The steel casing had an external diameter of 50.8 mm and a wall thickness of 3.2 mm. The casing diameter was selected based on the internal dimensions of the autoclave used for enhanced curing, ensuring it could accommodate five samples per height, arranged in a star-like pattern with four along the edges and one in the centre. The use of mild steel casing (Grade CFS 3BK) instead of super duplex steel (used typically for CCS well) was sought by the project consortium at the onset of the project to allow for possible occurrence of corrosion to take place, in addition facilitating the machining of the two ends of the tube.

At the outset of the project, steel casing samples of varying lengths (25 mm, 50 mm, and 70 mm) and diameters (30.8 mm and 50.8 mm) were evaluated to determine their impact on bond strength, failure mechanisms (either shear sliding or sealant crushing), and the maximum load in relation to the capacity of the test machine. These tests were conducted under controlled laboratory conditions at 20^{o}C and ambient pressure, with specimens cured for a duration of 90 days. Following these initial tests, the 50 mm length was chosen, as illustrated in the schematic in **Figure 2**. This selection struck a balance by reducing fabrication errors associated with shorter specimens (25 mm) while ensuring that failure occurred due to shear sliding rather than crushing. Furthermore, the applied loads were well within the capacity of the test machine, ranging from 9.0 kN for 25 mm samples to 16.1 kN for 50 mm samples, and reaching 28.8 kN for 70 mm samples. This provided adequate margins for testing the primary specimens cured under elevated curing. As the main samples underwent enhanced curing (details provided below) and were anticipated to demonstrate significantly higher strength, the decision was made to proceed with the 50 mm sample length.

Figure 2. Schematic of test sample representing a miniature of a plugged wellbore

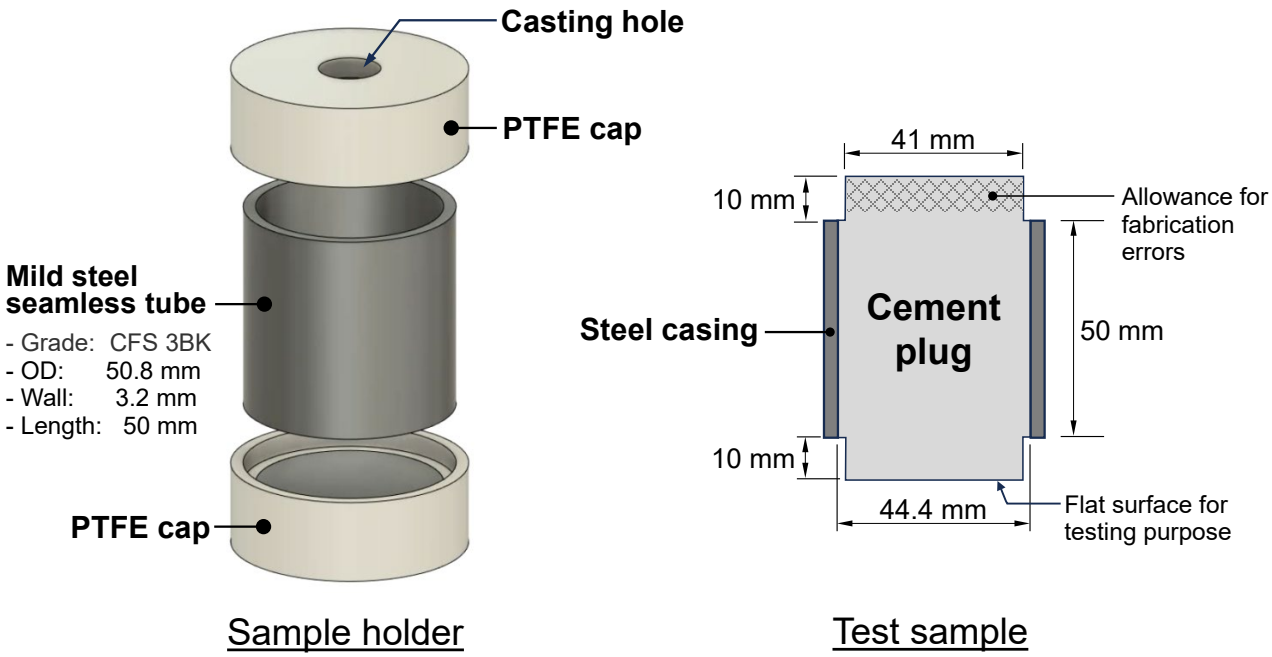

The internal sealant cement plug measured approximately 44.4 mm in diameter and had a 10 mm protruding section at each end with a diameter of 41 mm. These protruding ends were designed to minimise boundary effects during mechanical bond testing. The top protrusion addressed potential issues caused by uneven surfaces and lower-quality material at the top during sample preparation, while the bottom protrusion was provided to minimise stress concentrations during testing. This protruding shape was achieved using two PTFE end caps that enclosed the sealant during fabrication and curing. The top PTFE cap included a 20 mm central hole to facilitate casting, whereas the bottom cap remained unmodified, providing a flat surface suitable for bond testing.

Samples designed for electrical measurements were equipped with embedded electrodes to facilitate data collection. During initial trials, a vertical arrangement of stainless-steel rings positioned along the centreline of the samples was utilised. It was observed that this electrode configuration imposed excessive restraint on the sealant during high-temperature curing, resulting in the formation of significant radial cracking in the sealant material, which rendered the samples produced for further testing. Consequently, the electrode design was modified to mitigate these issues. The final electrode design employed two miniature electrode configurations: the 2-pin parallel pair and the 1-pin coaxial, **Figure 3**. The electrodes were significantly smaller relative to sample size to minimise restraint, thereby reducing the likelihood of cracking during high temperature curing. In the 2-pin parallel-pair configuration, two marine grade steel rods, each 2.4 mm in diameter and spaced 15 mm (centre-to-centre), were positioned along the full length of the sample, to obtain its bulk electrical properties. Conversely, the 1-pin coaxial configuration utilised a single 2.4 mm diameter rod positioned along the centreline of the sample as the first electrode, with the steel casing serving as the second electrode. This coaxial configuration enabled impedance measurements through the sealant material and at the sealant/casing interface, thereby facilitating its assessment.

Figure 3. Schematic of 2-Pin (left) and Coaxial (right) electrode configurations

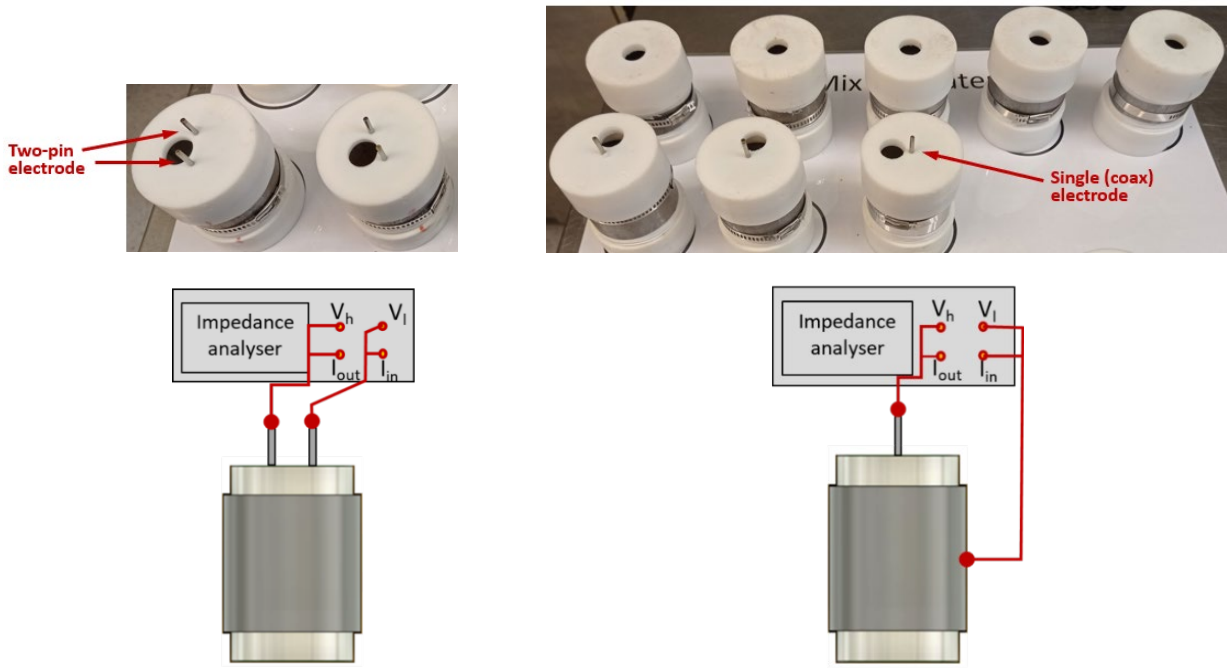

4.2.2 Sample Fabrication and Curing

Prior to the fabrication of the main test samples, each steel tube was cut to a length of 50 mm and immersed in a water-based degreasing solution for 24 hours. The inner and outer surfaces of the tubes were thoroughly wiped using paper towels, and this process was repeated to ensure complete removal of any oils remaining on the inner surfaces from the cutting and milling processes. Once fully cleaned, the steel tubes were transported to Norway for sample fabrication. For each sealant material, a total of 14 samples were prepared: six for bond testing to assess shear bond strength, six for electrical testing to measure impedance and conductivity, and two held as spares. All mixes were produced by the technical team at Halliburton in Norway following API Recommended Practice 10B-2, with casting carried out immediately thereafter by HWU staff. Sealants S1 and S2 were fabricated on the same day, as were Sealants S3 and S4. Sealant S5 was manufactured alongside repeated batches of Sealants S4 and S1. Consistent sample preparation methods were employed for all sealants to ensure valid comparisons could be made. Additional samples of Sealant S1 were produced in the UK, as this was the only non-proprietary sealant mix included in the study. These samples allowed for further investigation into factors affecting test results, providing greater insight into the variables impacting sealant performance under simulated wellbore conditions.

With regards to curing, as illustrated in **Figure 4**, this was conducted using an autoclave to expose the test samples to elevated temperatures and pressures shortly after fabrication, within 30 – 45 minutes of gauging with water. Two distinct curing media were utilised: water for most of the samples and oil for two samples with the 2-electrode configuration, enabling the monitoring of bulk electrical responses during the curing process. The autoclave system was pressurised to 300 bars (equivalent to approximately 3000 metres below sea level), and the internal temperature was increased gradually over 4 hours from 20°C to 80°C, where it was maintained for 3 days. This temperature of 80°C was chosen as it reflects the minimum CCS operational temperature and ensures practicality during bond testing. Subsequently, the

temperature was raised from 80°C to 150°C over 7 days and held at 150°C for an additional 21 days. At the end of this (31.33-day period under pressure), the temperature was steadily reduced from 150°C to 20°C over 7 days. During this cooling phase, once the temperature reached 100°C, the internal pressure was released, allowing the chamber to stabilise in terms of pressure and temperature.

Figure 4. Schematic of 2-Pin (left) and Coaxial (right) electrode configurations

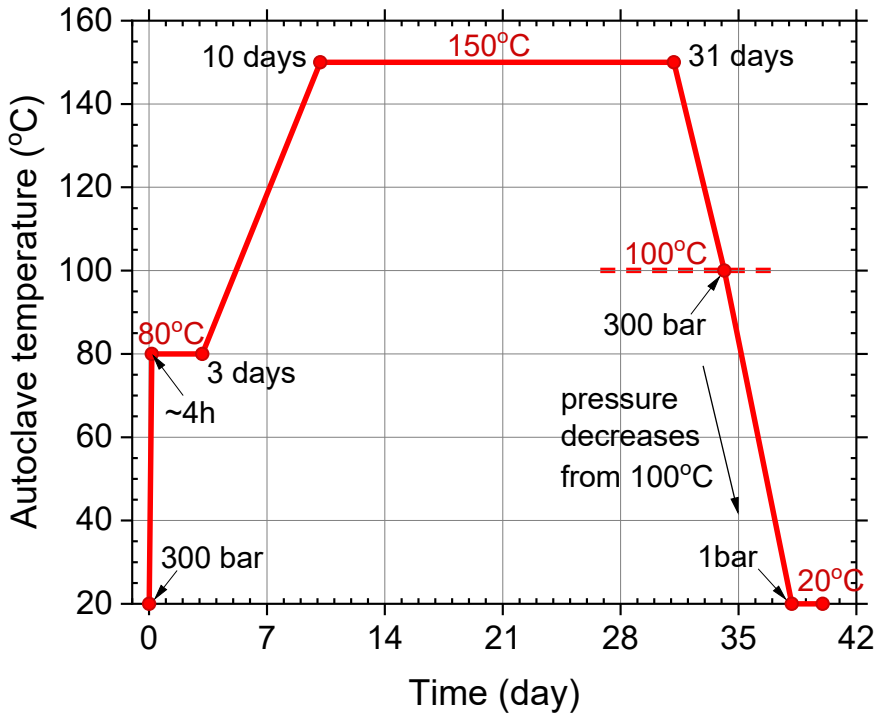

Throughout the high-temperature curing process, resistance data was recorded at 30-minute intervals to monitor the hydration and hardening of the sealant. Upon completion of the curing regime, all samples were submerged in water, covered with wet hessian cloth, and secured in sealed plastic containers for air transportation from Norway to HWU in the UK. Once received, the containers were stored at a controlled laboratory temperature of 20±1°C until the samples were required for testing.

4.2.3 Electrical Measurements during Curing

Once the slurry was sealed in the casings, the samples were placed in autoclave chambers filled with an aqueous containment fluid. For each sealant type, two samples equipped with the 2-pin electrode configuration were connected to a logging system designed to monitor in-situ low-frequency resistance (i.e., direct electrical current) during the curing process. As previously mentioned, these samples were housed in a separate chamber containing an electrically inert mineral oil containment fluid to prevent contamination of the electrical measurements. A bespoke logging system was employed, comprising a programmable logger that generated a square wave measurement voltage of 1 V peak-to-peak, recording the Resistance value from each sample. The logger was connected to the samples via a multiplexer unit capable of handling up to 72 individual measurements per measurement cycle. **Figure 5** depicts the logger and multiplexer units, the autoclave system, and the 2-pin electrode samples prepared

for containment within the autoclave chambers. Each sample was connected using thin lead wires interfaced with the multiplexer through a specialised 8-wire feedthrough connector.

Figure 5. Logging system placed above the two-chamber autoclave (left) and 2-pin electrode samples ready for testing (right)

4.2.4 Shear Bond Testing

One day prior to bond testing, all samples were pre-conditioned in an environmental chamber to gradually raise their temperature back to 80ºC over a 24-hour period. During this phase, the samples were submerged in water to stabilise the temperature and prevent moisture loss from the samples.

The bond tests were conducted using a 100 kN Instron 5892 testing machine. The experimental setup, schematically depicted in **Figure 6**, followed the procedures outlined in Patent No NO20191422 (US11054353B2). However, adjustments had been made earlier to facilitate the curing of test samples under elevated temperature and pressure, as described previously, to prevent crack formations that could compromise the integrity of the samples for further testing.

Before each test, the samples were removed from the chamber and wrapped tightly with 30 mm-thick pipe insulation to minimise heat loss. Each sample was then placed in an upside-down position on a central-hollow steel bracket (pre-conditioned to 80ºC), ensuring the flat face of the sample faced the loading plate. A hemispherical steel plate was used to apply the load in a controlled manner at a rate of 5 kN/min.

The testing machine automatically halted when a significant drop in resistance (greater than 20%) was detected, typically caused by either the sliding or crushing of the inner cement plug. Each test lasted approximately 5 to 10 minutes, which can be categorised as quasi-static in nature.

Figure 6. Schematic diagram of bond test

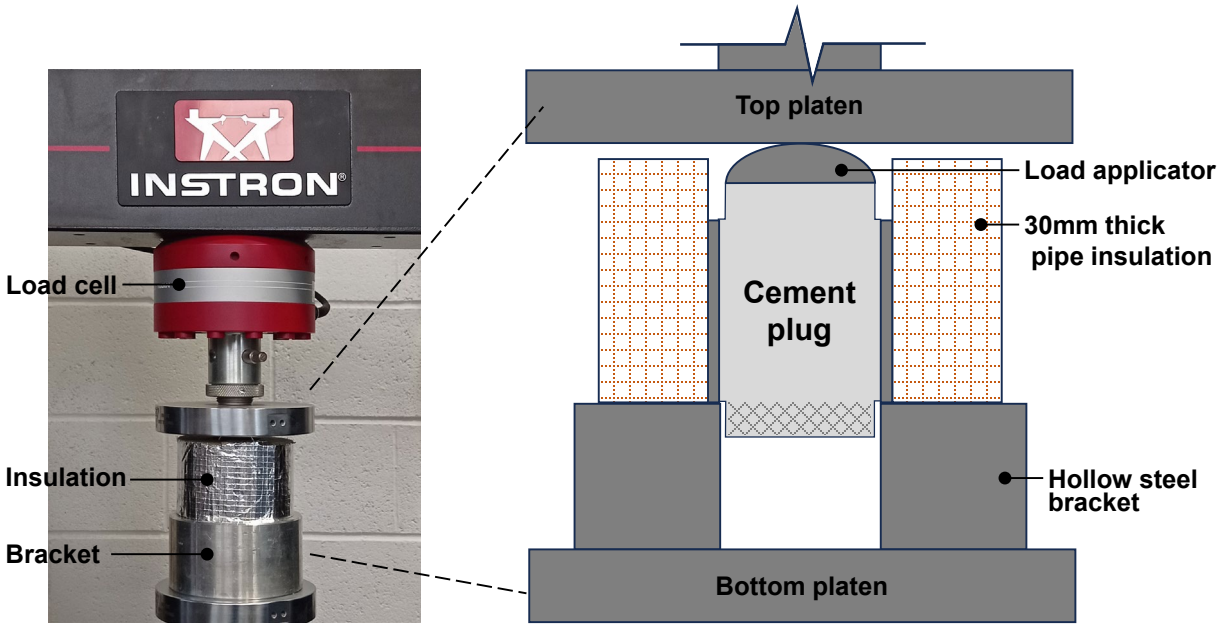

The apparent mean bond stress, τ (MPa), during testing can be calculated as

$$\tau = \frac{P}{A} \qquad \text{Equation (1)}$$

where P is the applied load (in N) and A is the contact area between the sealant and steel casing (approximately 44.4 × 50 mm^2).

4.2.5 Exposure Test: Accelerated Corrosion

The formation of corrosion products within confined spaces, such as the sealant/casing interface, can lead to the development of internal confining stress due to the expansive nature of corrosion. This can, in turn, enhance bond strength. To investigate the influence of confining stress on bond strength, two series of additional tests were undertaken.

In the first series, test samples were fabricated under standard laboratory conditions, at a temperature of 20^{o}C and normal atmospheric pressure. The second series involved fabricating test samples under enhanced temperature and pressure conditions, as previously applied. Accelerated corrosion tests were carried out on the samples to evaluate their corrosion potential and bond strengths after exposure. The purpose of the initial series was to identify suitable current levels and replicate the conditions of sealant S1 following enhanced (autoclaved) curing, during which significant corrosion was observed. These tests were conducted on the S1 sealant, referred to as LabCorr samples. The second series of tests included all sealants and is referred to as CemCorr samples.

A schematic diagram of the accelerated corrosion tests and the corresponding samples is presented in **Figure 7**. Each sample contained 2.4 mm diameter stainless-steel rod embedded along the longitudinal axis of the sample at the time of casting. These samples were stored under water for 25 days. As illustrated in the schematic diagram, the lower part of the samples was immersed in water in a small plastic container. On the same day (Day 26), four of the

samples were connected to a DC power supply to artificially induce corrosion. This was done by connecting the stainless-steel central rod to the positive terminal of the power supply (acting as a cathode) and the metal casing to the negative terminal (acting as an anode). Two of the samples were exposed to a constant current of 15mA and the other two to 30 mA, corresponding to an average current density of 0.21 and 0.42 mA/cm2, respectively. They were connected to the power supply for 6 days, followed by 1 day rest to allow for various measurements to be undertaken. This continued on a weekly basis until required for bond testing at 90 days. The remaining three samples were left unconnected and used as a benchmark. During the testing period, half-cell potential measurements were taken (between the stainless-steel rod and the mild-steel casing) to evaluate the likelihood and presence of corrosion.

Figure 7. Photo and schematic diagram of accelerated corrosion exposure test

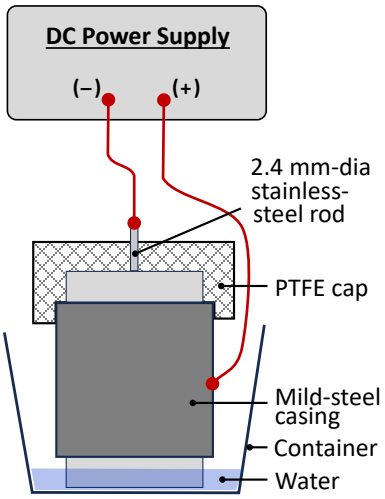

4.3 Results and Discussion

4.3.1 Electrical Measurements during Enhanced Curing

The resistance of the sealants is expected to be thermally activated, exhibiting a negative temperature response, meaning that resistance decreases as temperature rises. However, during the early stages of curing, both before and after setting, the resistance of the sealants is influenced by competing factors. These include changes in microstructural characteristics (and consequently the availability of conduction paths) as well as variations in the ionic content of the pore solution (and therefore its conductivity).

Figure 8 illustrates the resistance profiles of all sealants during the enhanced curing process, alongside the corresponding temperature profile. Referring to the response of Sealant S1 in the top section of **Figure 8**, resistance gradually increased over the first 3 days at 80^{o}C, indicating the early development of a pore structure due to Portland cement hydration (Stage I). This trend was briefly reversed as the temperature began to rise (Stage II), with resistance decreasing in response to the thermal effects described above. However, as the temperature

continued to increase, accelerated hydration and further pore structure development reversed this trend, leading to a renewed increase in resistance (Stage III).

The rate of resistance increase became more pronounced at approximately 130ºC (Stage IV) and further at 150ºC (Stage V), likely reflecting the active involvement of silica flour in the hydration process. At the constant temperature of 150ºC, resistance continued to increase at a slower pace, demonstrating ongoing microstructural development as hydration progressed. Towards the end of Stage VI, resistance appeared to stabilise, indicating near or full hydration. After approximately 31 days, the temperature was steadily reduced from 150ºC to 20ºC over a controlled period. During this cooling phase, when the temperature reached 100ºC, the resistance of the cured samples increased significantly, reflecting their negative temperature response, before eventually plateauing (Stage VIII).

Figure 8. Resistance profile for Sealant S1 (top) and Sealants S2–S5 (bottom) during enhanced curing

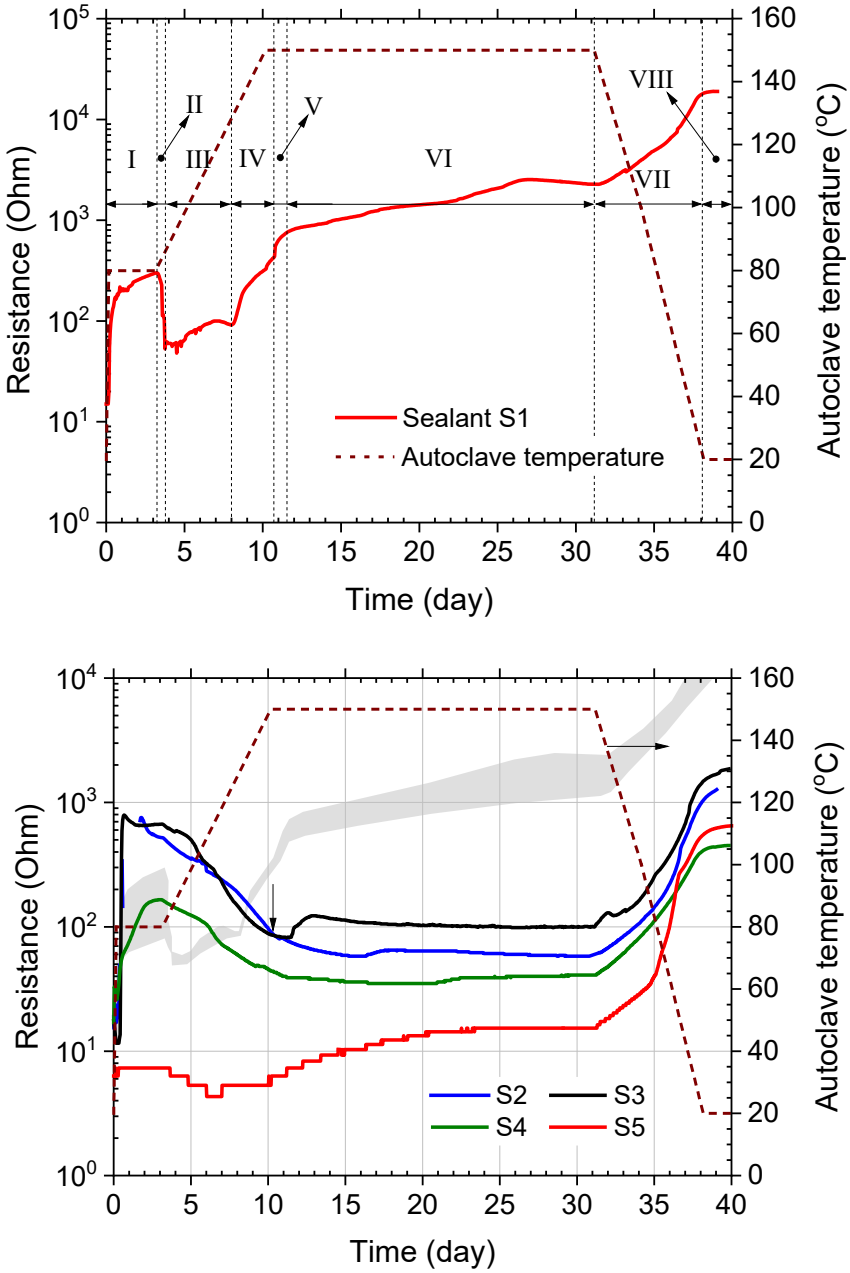

The resistance profiles of Sealants S2, S3, S4, and S5 are presented in **Figure 8 (bottom)**, alongside the autoclave temperature profile and the resistance variation for Sealant S1 (illustrated in the shaded grey area). Similar to Sealant S1, the resistance of these sealants was found to correlate with temperature throughout the curing process. However, each sealant exhibited distinct resistance values and unique characteristics as hydration reactions advanced. These variations at critical stages are attributable to the specific materials and additives incorporated within each sealant.

For instance, Sealants S2 and S3 displayed comparable curing profiles during the initial stages, marked by a rapid rise in resistance approximately 6 hours after the temperature reached 80°C. While the temperature remained constant at 80°C (Stage I), the resistance of Sealant S2 began to decline, likely due to material dissolution. In contrast, Sealant S3 maintained steady resistance levels, which may indicate the activation and dissolution of the ReStone® mineral component in its hydration process. During the temperature increase from 80°C to 150°C, both sealants exhibited a consistent decline in resistance. Sealant S3 experienced a brief, sudden rise in resistance around 29 hours after reaching 150°C, which quickly stabilised, potentially signifying further involvement of the ReStone® mineral component in the hydration process.

Sealant S5, the one-part geopolymer, demonstrated the simplest behaviour among the sealants. It showed no significant change in resistance while the temperature was held at 80°C during Stage I, reflecting the competing influences of material dissolution and pore formation at this early stage. As the temperature increased towards 150°C, resistance initially declined as expected due to thermal effects. However, this trend reversed after 7 days when the temperature approached 120°C, at which point resistance began to increase. This indicates the precipitation of materials, with a pore structure gradually being filled by precipitating hydration products. The upward trend in resistance continued until day 23, after which it stabilised as curing neared completion.

Finally, all sealants exhibited a pronounced rise in resistance as the temperature decreased from 150°C to 20°C at the end of the curing process. This increase was driven by temperature effects on conductivity. However, the distinct rates and profiles observed for each sealant suggest unique thermal activation characteristics, which will be examined further in the subsequent discussion.

4.3.2 Mean Bond Strength and Stiffness

Figures 9(a)–(c) illustrate the mean bond stress versus top displacement relationships for the initial four sealants, with each figure comparing data from three nominally identical samples for each sealant to those of Sealant S1. Results for Sealant S5 are detailed in the subsequent section, as this batch was tested during the later stages of the project using a different reference. Overall, the comparisons show that all sealants exhibited a similar pattern of increasing mean bond stress with displacement until failure, which occurred abruptly due to vertical sliding of the sealant.

The data in **Figures 9(a)–(c)** reveal variations in bond strength and overall stiffness across the different sealants, with the order of these properties decreasing as follows: S1 > S3 > S2 > S4. For example, Sealant S2 samples had mean bond strength and stiffness values of 1.51 MPa and 8.95 N/mm^3, which equate to only 32.5% and 80.6% of the values for Sealant S1, respectively. In comparison, Sealant S3 samples demonstrated higher performance, with mean bond strength and stiffness of 3.54 MPa and 9.20 N/mm^3, corresponding to 75.9% and 82.9% of the reference values. Sealant S4 exhibited the lowest mean bond strength and stiffness among the sealants, with values of 0.54 MPa and 2.88 N/mm^3, respectively. These figures represent only 11.5% and approximately 26% of those for Sealant S1. This performance may be attributable to sliding shear movement between the sealant and the steel casing during testing.

Figure 9. Mean bond stress–top displacement for Sealants S1–S4

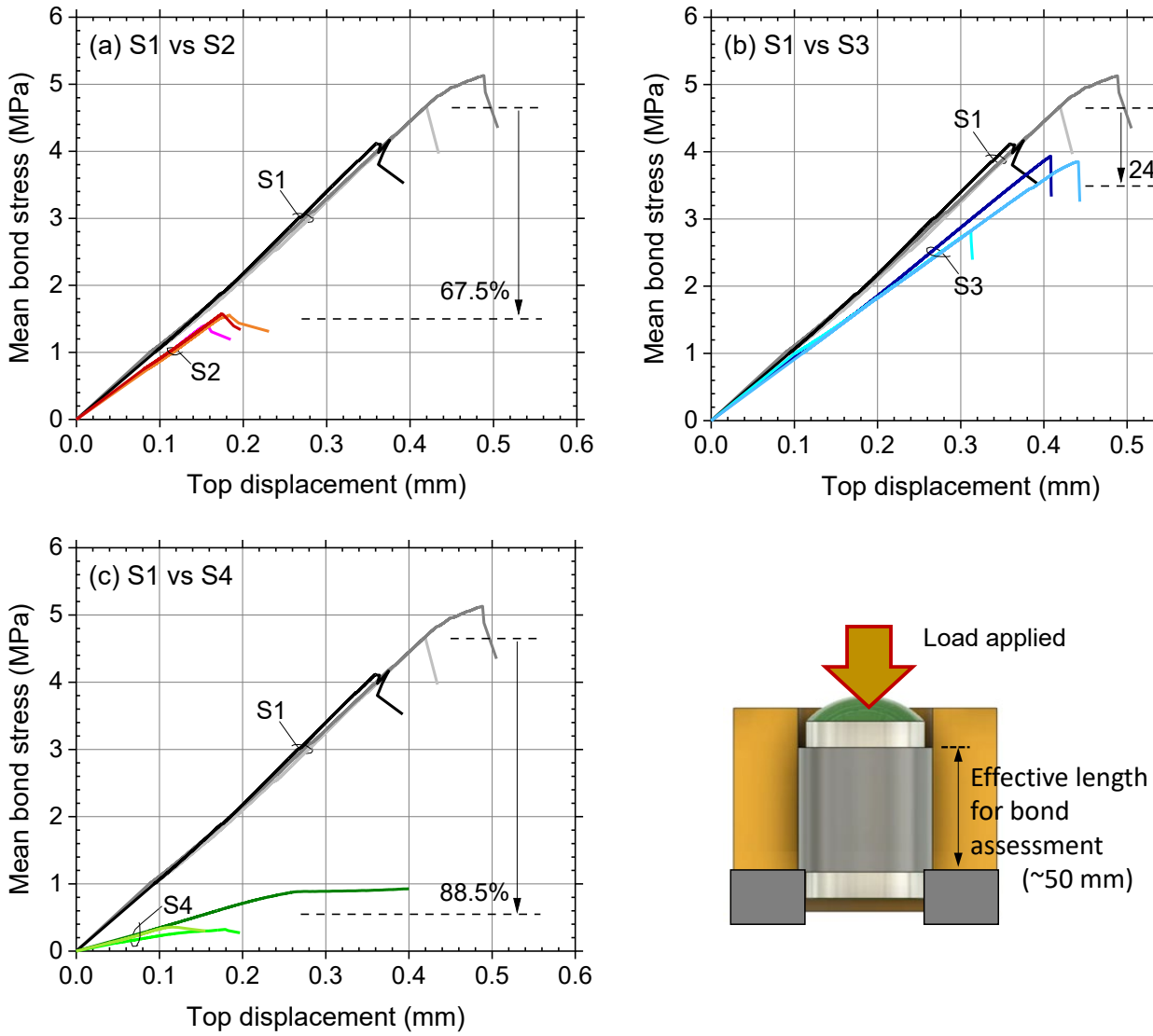

Direct comparisons of the mean bond strengths reported in previous studies are challenging due to the limited availability of published data, as most samples were cured under ambient or low-pressure conditions. Nevertheless, some comparisons are presented in **Figure 10(a)**. Notably, the mean bond strengths of Sealants S2 and S4 fall within the range of reported values, while those of Sealants S1 and S3 tend to be higher. Interestingly, the mean bond

strength of Sealant S2 samples (1.51 MPa), which includes an expansive agent, is similar to the 1.5 MPa average recently reported by Kamali *et al.* (2022) for cement test samples containing a magnesium oxide expansive agent. In contrast, the mean bond strength of Sealant S1 samples (4.66 MPa) is significantly higher than the 0.6 MPa average from the same study, which was measured on Portland cement (Type G) encased in metal casing and cured in a 90°C chamber at 34 bars for only 7 days.

Additionally, **Figure 10** illustrates that the mean bond strength of Sealant S1 samples exceeds the reported range of 1.4 – 3.1 MPa for metal pipes encased in sealant, as well as the 0.12 – 0.26 MPa range reported by Mabeyo *et al.* (2020) for cement samples encased in cement mortar and cured in an 80°C water bath at ambient pressure over 28 days. It is therefore plausible that the lower bond strengths observed for Sealants S2 and S4 in **Figures 9(a) and (c)** are not indicative of reduced performance but rather reflect the elevated bond strengths of Sealants S1 and S3.

In addition to bond strength, the apparent stiffness derived from the shear bond test is also worth analysing. The overall stiffness is influenced by factors such as deformation of the top protruding section of each sample during loading, initial slip between the sealant and metal casing, and deformation of the entire test setup which can be expected to be similar across all samples. Comparing the stiffness values of each sealant with their modulus of elasticity (MOE) can therefore offer insights into the extent of initial slip experienced during bond testing.

Figure 10. Comparisons of bond test results with basic mechanical properties

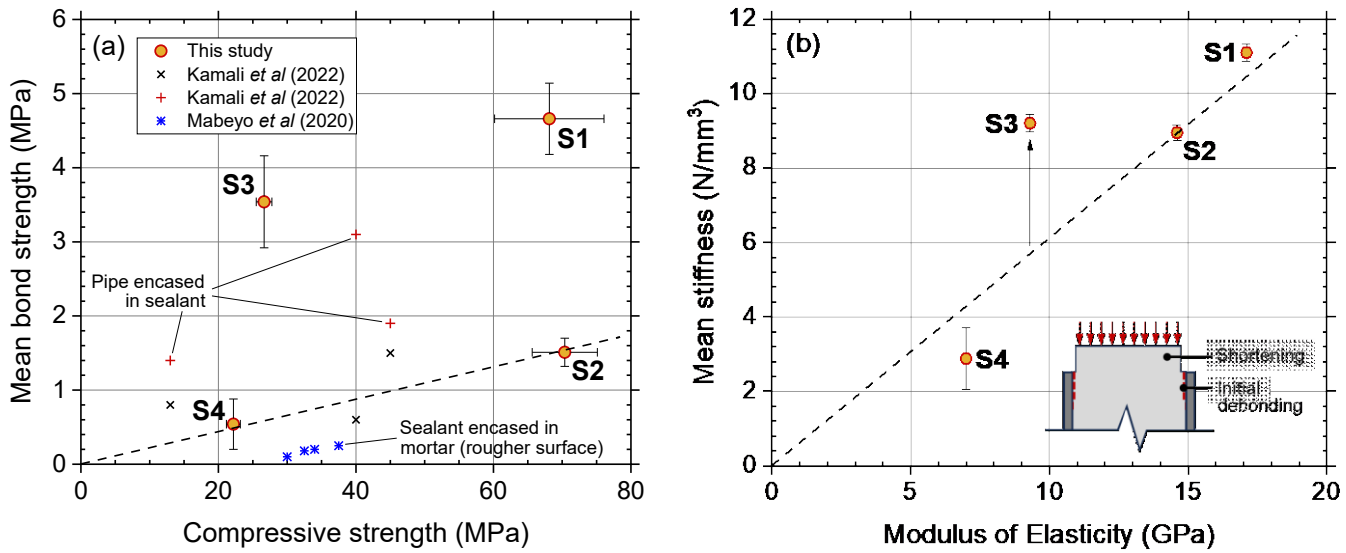

Figure 10(b) provides a comparison of the overall stiffness obtained from each sample plotted against their respective MOE value. It should be noted that the MOE for each sealant was measured in WP 1 on nominally identical materials, which were cured at 150°C and 300 bar for 28 days, resulting in compressive strengths of 107, 76, 32, and 21 MPa for Sealants S1 through S4, respectively. The figure demonstrates an almost linear correlation between the overall stiffness obtained from bond testing and the MOE of the sealants. Sealant S3 represents an exception to this trend, as it exhibited higher stiffness than what would be predicted by the linear relationship (as indicated by the arrow). This suggests that Sealant S3 may have experienced less sliding during bond testing compared to the other sealants.

Conversely, Sealant S4 displayed slightly lower stiffness than the trendline average, which may indicate a comparatively greater degree of initial slip during testing, but the extent was not particularly significant. To investigate the contributing factors further, the internal sealant plug was extracted from the metal casing after testing, and this is examined in the following discussion.

4.3.3 Inner Surface Condition and Failure Mechanisms

Following the completion of bond testing, each sample underwent machining to extract the internal cement plug from the steel casing for visual inspection of the sealant/steel casing interface. This was achieved by milling the outer surface of the steel casing to create a longitudinal recess, gradually cutting through the full thickness of the steel. Once this process was complete, the cement sealant was removed and photographed.

Photographs were captured by placing each sealant sample at a fixed distance from a DSLR camera and rotating the sample to take multiple shots. Twelve images were acquired for each sample to ensure sufficient overlap for stitching. The images were subsequently corrected for distortion using Adobe Photoshop and combined into a single composite image using the Photomerge function.

Figure 11 presents the resulting images from the sealant samples. Sealant S1 exhibited significant corrosion products across its entire surface, predominantly in dark brown and black colours. Small patches of the original sealant surface were visible where the rust layer had detached during the extraction or milling process, as can be seen on the right-hand side of the Figure.

Sealant S2 revealed an intriguing surface pattern characterised by small white or light-grey patches scattered across a darker grey background. Upon examination, the white or light-grey zones were identified as material that had adhered directly to the steel surface but separated under loading. The darker background represented the exposed subsurface of the sealant material immediately beneath the sealant/steel interface. This resulted from the detachment of the still-adhering sealant surface from the sample body. Therefore, it can be inferred that the bond failure of Sealant S2 samples was a combination of material failure beneath the steel-material interface and partial failure of the sealant/steel bond.

Sealant S3, similar to Sealant S2, exhibited only minor corrosion concentrated at the ends of the sample. However, Sealant S3 displayed a clean surface typical of hardened cement paste in appearance and texture. As shown in **Figure 12**, the inner surface of the steel casing was relatively clean, with minimal corrosion. This suggests that the failure of Sealant S3 samples was predominantly due to bond failure at the sealant/steel interface.

Sealant S4 exhibited moderate corrosion, appearing brighter in colour compared to that observed in Sealant S1, along with signs of a failure surface where a layer of sealant material near the interface had spalled off. Apart from these specific areas, the remaining surface was relatively clean, resembling the texture of hardened cement matrix similar to that of Sealant S3 samples. Similar patches of corrosion were also visible on the inner surface of the steel casing.

Figure 11. Montage of the sealant surface post testing

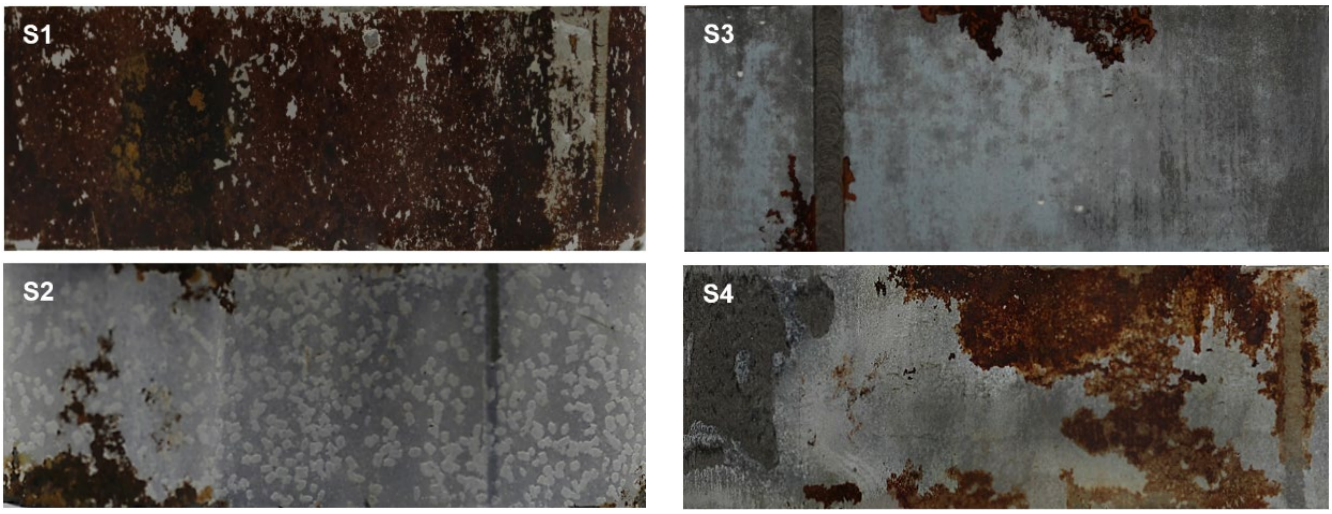

Figure 12. Surface condition of the inner pipe post bond testing

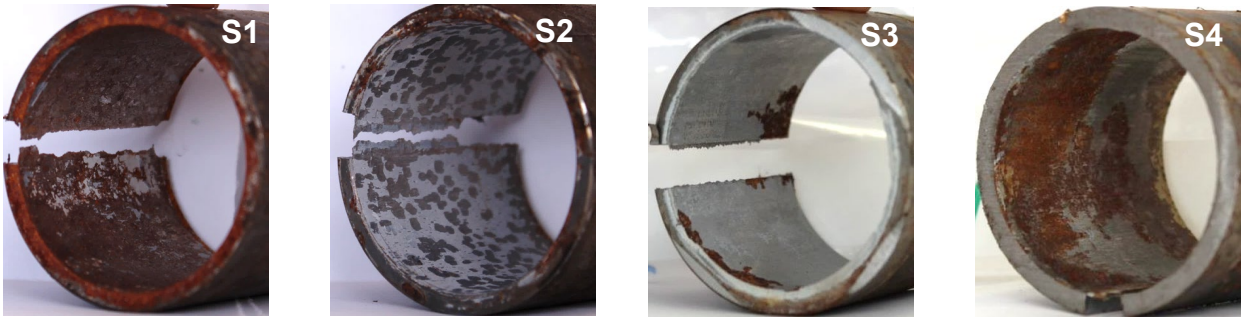

4.3.4 Post Exposure Bond Strength: Effect of Corrosion

Figure 13 displays the 90-day mean bond stress vs top displacement relationships for the three groups of S1 sealants, with the tests performed at 20°C and under a crosshead speed of 0.2 mm/min. It is evident that there is a noticeable difference in bond performance between the three groups of samples in terms of bond strength and overall stiffness. In general, an increase in the 90-day mean bond strength with increasing current levels is evident, from 0.91 MPa at 0 mA to 1.19 MPa at 15 mA (or 30.8% increase) and 3.18 MPa at 30 mA (349% increase). This confirms the above postulate that the enhancement in bond strength is affected by the extent of corrosion at the sealant/casing interface.

Further evidence of the effect corrosion was obtained from the second series of CemCorr samples. For the primary sealants, it was observed that the mean bond strengths following extended corrosion exposure were consistently higher than those recorded prior to corrosion. Extensive corrosion formation was evident at the sealant/steel casing interface in all sealants, caused by the application of electrical current during the accelerated corrosion process. Sealant S2 samples demonstrated the most pronounced increase in bond strength, rising markedly from 1.51 MPa to 5.98 MPa. This significant enhancement could be attributed to the high modulus of elasticity of this sealant, which may have led to substantial internal confining stress resulting from the expansive corrosion at the interface. Sealant S4 samples, as before,

exhibited the lowest mean bond strength of 0.91 MPa, yet this still represented a noteworthy improvement from its pre-corrosion value of 0.51 MPa. Sealant S1 samples displayed considerable variability in bond strength, influenced by significant differences in corrosion levels across individual test specimens. The mean bond strength for Sealant S1 was recorded at 9.3 MPa, surpassing its previous value of 4.7 MPa. Sealant S3 samples also showed an increase, with a mean bond strength of 3.75 MPa, compared to the pre-corrosion value of 3.54 MPa. The increase was more modest, likely attributable to the lower modulus of elasticity of Sealant S3, which would result in reduced additional confining pressure.

Figure 13. Results of bond test on samples exposed to accelerated corrosion

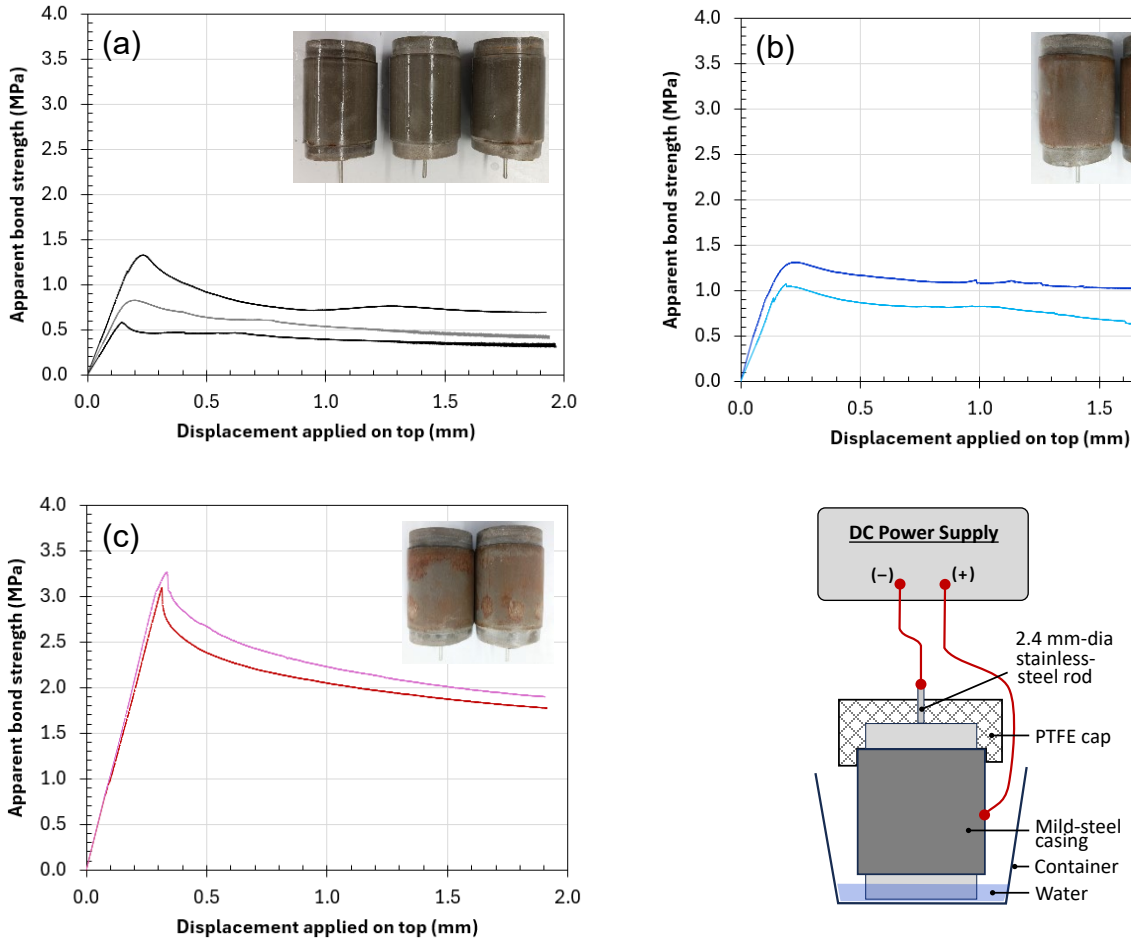

To provide additional insights into the effect of corrosion, three additional samples were cast: two using the same mild-steel tube casing and the other using stainless-steel mould. These samples were cured at enhanced temperature and pressure. They were also tested using the same test procedures, involving sample pre-conditioning and testing temperature of 80ºC. It was observed that corrosion at the interface resulted in elevated bond strength by 22–39%, further supporting the hypothesis regarding the secondary effect of corrosion on bond strength. While corrosion may temporarily elevate bond strength due to confining pressure, this effect is considered not permanent and is expected to diminish over time as the sealant undergoes creep and shrinkage. As such, the increased bond strengths measured in samples with corroded metal casing are considered artificial. Over time, the expansive nature of corrosion, combined with the sealant's creep and shrinkage, may lead to greater porosity within the corrosive layers forming on the inner casing surface as corrosion advances. Ultimately, this

porous layer could create leakage pathways. To mitigate this risk, it is strongly recommended to take preventive measure against corrosion by employing non-corrosive casings or sealants that have properties that can reduce the likelihood of corrosion initiation.

4.3.5 Effect of Setting Time

During the initial hours following gauging, cement slurry undergoes the setting process, during which it increases in rigidity and transitions from a liquid to a solid state. While direct measurements of the setting time were not carried out, observations revealed considerable variation in the setting times of the four sealants at ambient laboratory temperature, increasing in the order: Sealant S4 (less than 30 minutes) < S2 (approximately 45 minutes) < S3 and S1 (more than 1 hour). Interestingly, this sequence corresponds to the order of mean bond strengths obtained for the sealants.

Cement slurry with a faster setting time is expected to solidify more rapidly, particularly under conditions of rapid temperature increase. This is simulated in this study by the initial rise from 20^{o}C to 80^{o}C over 4 hours. It is anticipated that accelerated hardening may compromise the bond with the metal casing. Furthermore, despite high-pressure curing at 300 bar, in this work, the situation may have been exacerbated by the expansion of the metal casing during initial heating and the absence of lateral confinement typically provided by surrounding rock formations. In light of these, it was deemed necessary to investigate the effect of setting time. Testing for Sealant S4 was repeated to determine if its low bond strength was associated with its rapid setting characteristic. To address this, a retarding agent of unspecified type and quantity was introduced into the original mix to slow the initial reaction kinetics. The same testing procedures, including elevated curing temperatures and pressures, were employed as before.

Figure 14 compares the results of the original Sealant S4 with the modified Sealant S4R. Beyond the 6-day mark (above 110^{o}C), the profiles of both samples were largely similar, with S4R showing slightly lower resistance but remaining within the expected range of batch variations. This indicates that the expansive agent does not significantly affect the bulk properties of the sealant, especially in terms of pore connectivity. However, the addition of the retarding agent had a notable impact on the early stages, with Sealant S4R displaying significantly delayed and reduced resistance during the first 7 days, compared to the original Sealant S4. This demonstrates the distinctive effects of the retarding agent on the setting process and subsequent development of the pore structure during the initial curing stages. The impact on the later stages of curing appeared minimal, as reflected in the similarities between the two batches, including the slight increase around the 20-day mark and the steady final rise. This confirms that the primary influence of retarding agent lies in the early hydration stages.

Prior to bond testing, radial cracking was observed at the lower section of the sample protrusion above the casing. To enable testing, the sealant material was milled flush with the steel casing. The exact mechanism causing radial cracking, which may be linked to the retarding agent, is not fully understood but this might have resulted from the development of tensile stresses in the protrusion above the steel rim, due to restraint on volumetric changes of the sample during curing imposed by the steel casing.

Figure 14. Resistance profile of Sealants S4 (original) and S4R (repeat with retarding agent)

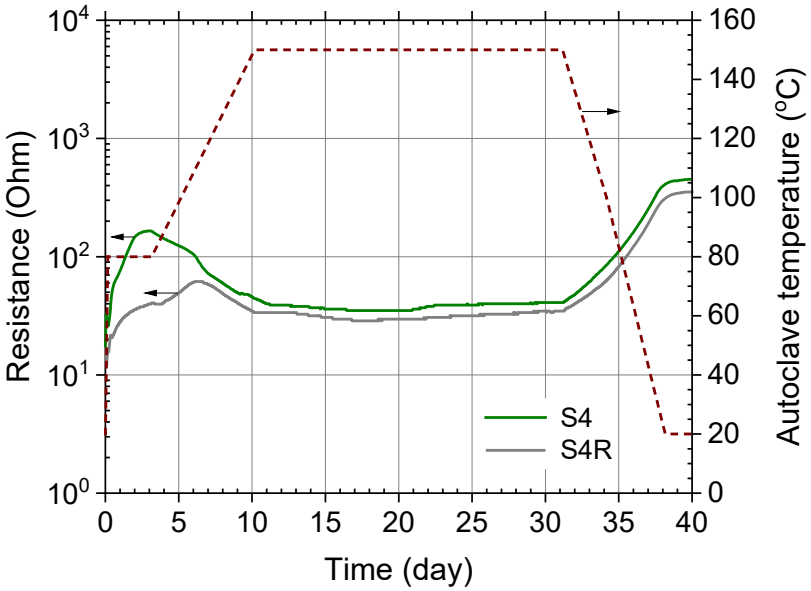

Figure 15 compares the mean bond strength from the repeat test (S4R) and the original test (S4). It is immediately evident that the repeat samples exhibited a significantly higher mean bond strength, averaging 5.45 MPa, thereby emphasising the advantage of slowing down the initial reactions to enhance bonding. Once the variation in the reference mean bond strengths between the two batches is accounted for, this represents an approximate five-fold increase. Interestingly, the failure mechanism for the repeat samples was dominated by the crushing of the sealant face beneath the loading applicator, rather than shear sliding at the sealant/steel interface as observed previously. After the bond tests, the metal casing was split open to examine the sealant and the inner surface of the casing, see **Figure 15**. A notable proportion of the sealant was found to remain adhered to the steel surface, further corroborating the high bond strength recorded. A moderate level of corrosion was still apparent, indicating that corrosion is influenced by the inherent characteristics of the sealant itself.

Figure 15. Bond performance of Sealant S4R with a retarding agent compared to Sealant S4 without a retarding agent, along with images of surface conditions post testing.

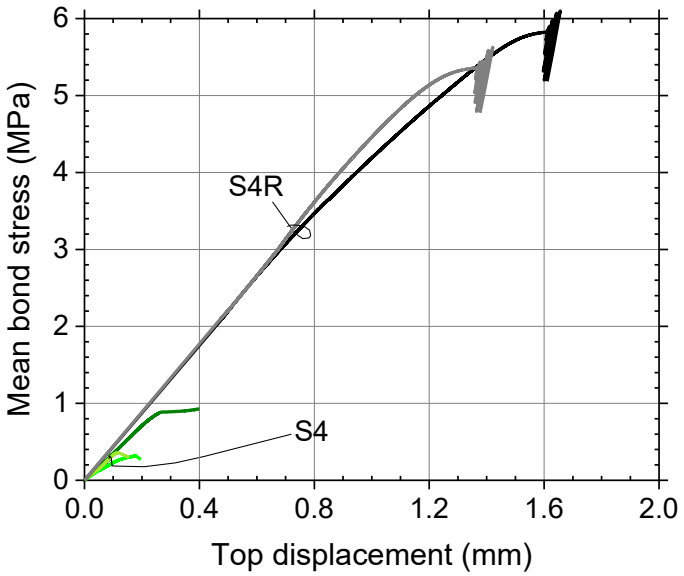

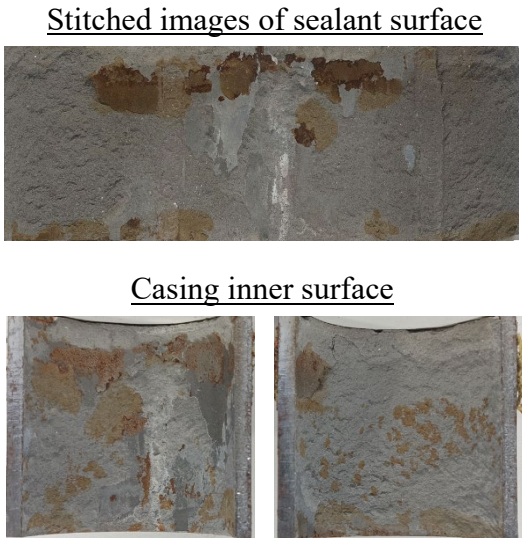

4.3.6 Effect of Curing Conditions

Cement hydration is governed by complex chemical reactions that are thermally activated. To ensure accurate evaluation, the curing and testing of CCS sealant materials should closely replicate the elevated temperature and pressure conditions present in a deep re-purposed oil or gas well.

Figure 16 provides a comparison of the mean bond strengths obtained from test samples cured under elevated temperature and pressure (up to 150°C and 300 bar over 38 days, labelled S1 and S1R) against those cured under standard laboratory conditions (20°C and atmospheric pressure over 28 days, labelled S1A). These values are plotted alongside their respective mean compressive strengths. It is worth noting that the S1R samples were encased in stainless steel casing, whereas S1 and S1A samples in mild steel. The beneficial impact of enhanced curing is clearly demonstrated by the bond and compressive strengths of samples cured under elevated conditions (S1 and S1R) compared to those cured under ambient conditions (S1A). Enhanced curing yielded an approximate twofold increase in compressive strength (ranging from ~35 MPa to 60–75 MPa), and an even more remarkable four- to fivefold increase in bond strength (ranging from ~0.9 MPa to 3.6–4.6 MPa). The elevated pressure (300 bar) applied during the primary curing regime must have promoted densification of the pore structure, thereby enhancing its compressive strength. Furthermore, elevated pressure helps to minimise volumetric changes, which contribute positively to bond strength. These factors explain the more substantial improvement observed in the mean bond strength.

Figure 16. Key properties of Sealant S1 cured under ambient and elevated curing

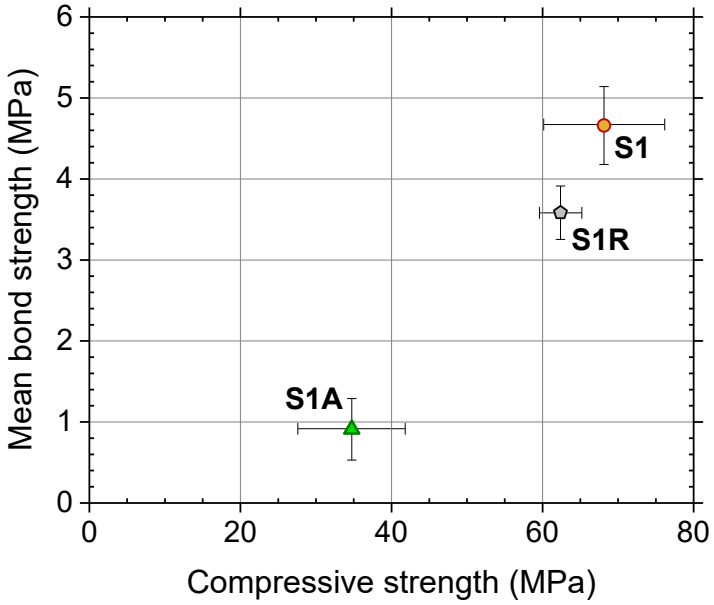

4.3.7 Bond Strength of Non-Portland based Sealant

Sealant S5 was the only sealant in this project that did not contain Portland cement. As its development took place during the early stages of the project, the fabrication of test samples for this series occurred later, during the final phase of testing. At this point, it was deemed necessary to produce Sealant S5 samples alongside Sealant S1RF (repeat final) as a reference. During this process, both mild-steel and stainless-steel casings were considered for

use. Due to significant differences in the fundamental composition of the two sealant materials, their curing processes were conducted in separate chambers to avoid any potential cross-contamination. This precaution was crucial, as Sealant S5 contained a high concentration of alkali activator, which could accelerate the hydration reactions of Portland cement and other supplementary materials. The samples underwent the same fabrication, curing, pre-conditioning, and testing protocols as the other four sealants.

Figure 17 presents the mean bond stress plotted against displacement, following the same format as previous data. Sealant S5 samples achieved a mean bond strength of 10.2 MPa, regardless of the casing material used (mild steel or stainless steel). In comparison, the repeat S1RF samples exhibited bond strengths ranging from 8.76 to 10 MPa, with an average of 9.4 MPa. These figures were more than double the average bond strengths recorded in previous batches and exceeded values reported in the published literature. The reasons for this significant increase in bond strength were unclear, but several factors might have contributed. Potential causes include inconsistencies in the oil removal process during preparation or errors in material batching. For example, the accidental addition of a retarding agent (known to enhance bond strength) or the unintentional inclusion of an expansive agent during batching. Additionally, transportation issues between Norway and the UK could have influenced the outcome, although such complications would typically reduce bond strength rather than enhance it.

Figure 17. Bond performance of (a) Sealant S5 and (b) Sealant S1RF (repeat).

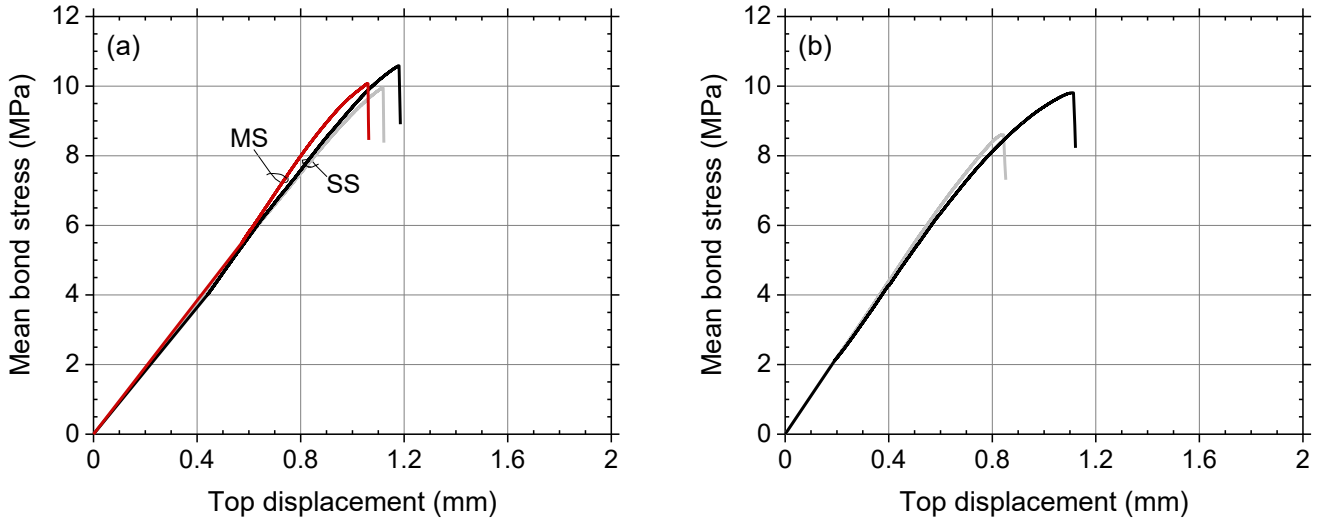

To investigate the above possibility further, impedance measurements were performed on the test specimens prior to the bond testing. The results, as shown in **Figure 18**, display a consistent response, indicating that the bulk electrical properties of the samples remain largely unchanged across the two batches. Consequently, any variations observed are likely attributable to factors associated with the sealant-casing interface. One possibility is due to the accidental inclusion of an expansive agent during material batching as the presence of such an admixture may not be evident in the impedance measurement results.

Figure 18. Comparison of the Impedance response of Sealants S1 (first 3 data sets) and S1RF (second 3 data sets)

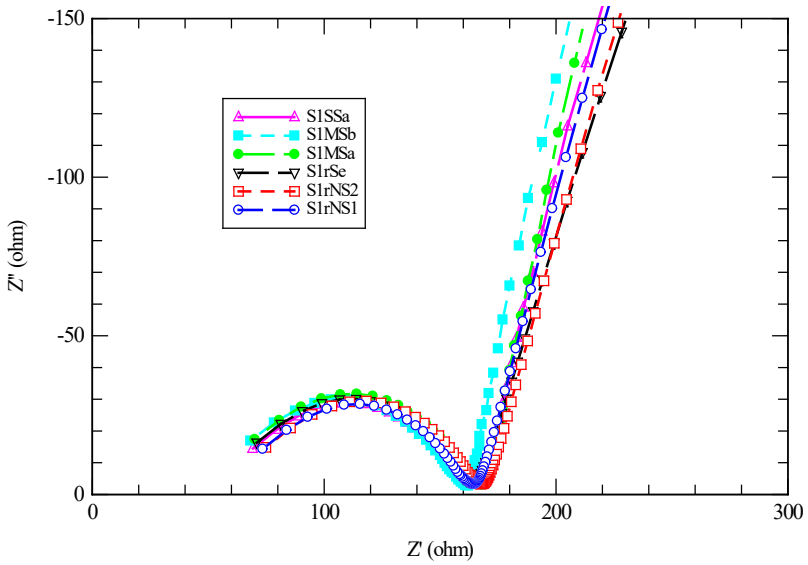

Figure 19 (a) displays the surface conditions of the Sealant S5 samples, illustrating both the outer surface of the sealant and the inner surface of the steel casing. Notably, this particular sealant demonstrates an exceptionally smooth interface with the steel casing, showing minimal and largely no visible signs of corrosion apart from a small, localised area highlighted in the figure. Among all the sealants tested in this study, Sealant S5 exhibits the smoothest surface, closely replicating the texture of the internal surface of the steel casing. From the photos, a discernible layering effect is visible, which suggests a degree of segregation occurred during the fabrication of the samples. This is likely due to the lower viscosity of Sealant S5 compared to the other sealants tested. The upper sections of the samples are lighter in colour and covered with numerous white spots, while the lower sections are darker but similarly exhibit several white spots.

For comparative purposes, **Figure 19(b)** presents the surface conditions of the Sealant S1RF samples, showing both the external surface of the sealant and the inner surface of the steel casing. Interestingly, no visible signs of corrosion are evident in these samples, a finding that contrasts with the results of the three previous batches. In this batch, the material near the surface appears to have sheared off, leaving white zones adhered to the steel surface. This suggests that this layer detached under the application of shear load. This observation indicates that the bond failure in the Sealant S1RF samples was governed by material failure below the steel/sealant interface rather than debonding. Although the exact cause of this behaviour could not be conclusively identified, the absence of corrosion in this batch could be attributed to enhanced volumetric stability compared to the original S1 sealant from earlier batches.

Figure 19. Conditions of the sealant's outer surface of and the pipe's inner surface following bond testing: (a) Sealants S5 and (b) S1RF.

(a)

(b)

4.3.8 Non-Destructive Testing

4.3.8.1 Post Enhanced Curing

During the post-curing phase, impedance spectra for all sealants were measured using a Solartron 1260 Impedance Analyser. These measurements were performed on samples of both coaxial 1-pin and parallel 2-pin configurations, which had been cured in a water medium within the autoclave. Data acquisition was conducted with a 1 Volt peak-to-peak excitation voltage across a frequency range of 1 Hz to 10 MHz, with 10 measurement points (in log) per

decade of frequency increment. **Figure 20** illustrates the frequency analyser alongside a connected sample.

Using parallel measurements, the sample-electrode geometric parameter, denoted as k, was calculated for both coaxial and parallel 2-pin sample configurations by comparing impedance results with those obtained from a Perspex cube sample holder. The derived values of the geometric parameter were k1p = 0.1568 and k2p = 0.1046 /m for the coaxial and parallel pair electrode configurations, respectively.

Figure 20. Solartron 1260 Impedance analyser with coaxial sealant sample

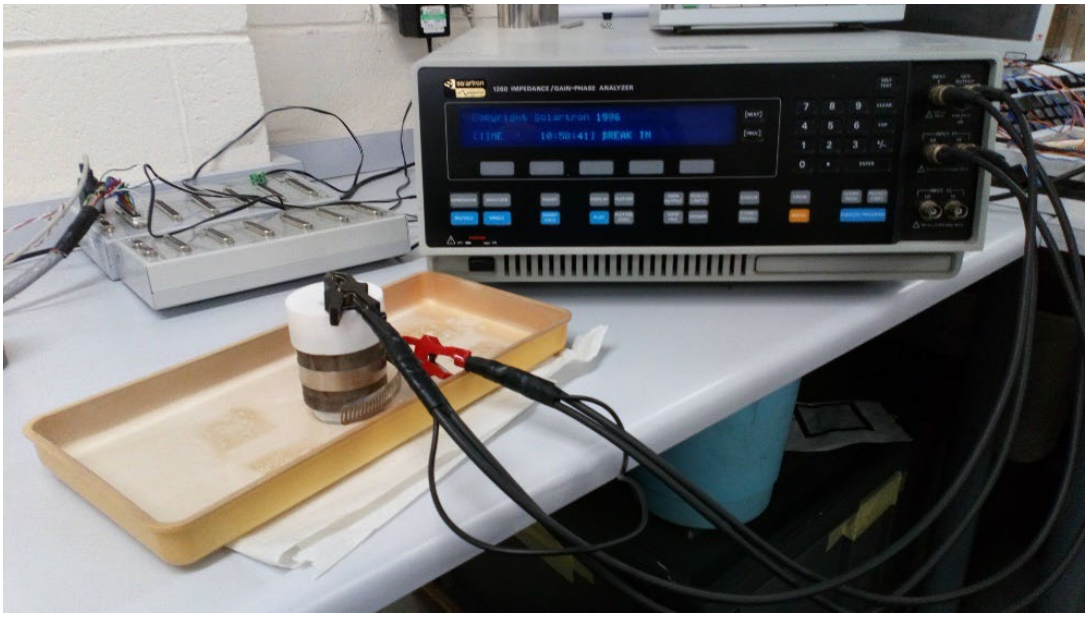

The processed impedance results for Sealants S1 through S5 are presented in **Figure 21** in the form of Nyquist diagrams, where Reactance is plotted against Resistance as the frequency increases from 1 Hz to 10 MHz. The impedance patterns for Sealants S1, S2, S3, and S5 exhibit a visually similar trend, progressing from right-to-left as the frequency increases. This trend features a long tail (or spur) and a depressed arc joined at a cusp point where the Reactance reaches its minimum. Specifically, this pattern resembles that observed for plain ordinary Portland cement.

The low-frequency tail of the response is influenced not solely by the material properties but significantly by the interaction between the material and the electrodes at their interface. In the coaxial configuration, this interaction extends to the sealant/casing interface. Notably, the absolute impedance values and frequency characteristics of this segment of the response vary among the sealants and differ by electrode type, particularly in the case of Sealant S5. Amongst the five sealants, the impedance response of Sealant S4 is particularly distinctive, as it exhibits a dual-arc feature rather than the single-arc feature observed for the other four sealants. This distinction can be attributed to the composition of this particular sealant, which is based on a calcium aluminate cementitious system and includes several proprietary additives. Similar dual-arc impedance features have previously been identified in Portland cement-based systems containing supplementary additions.

Figure 21. Post-curing Impedance plots of Sealants S1–S5

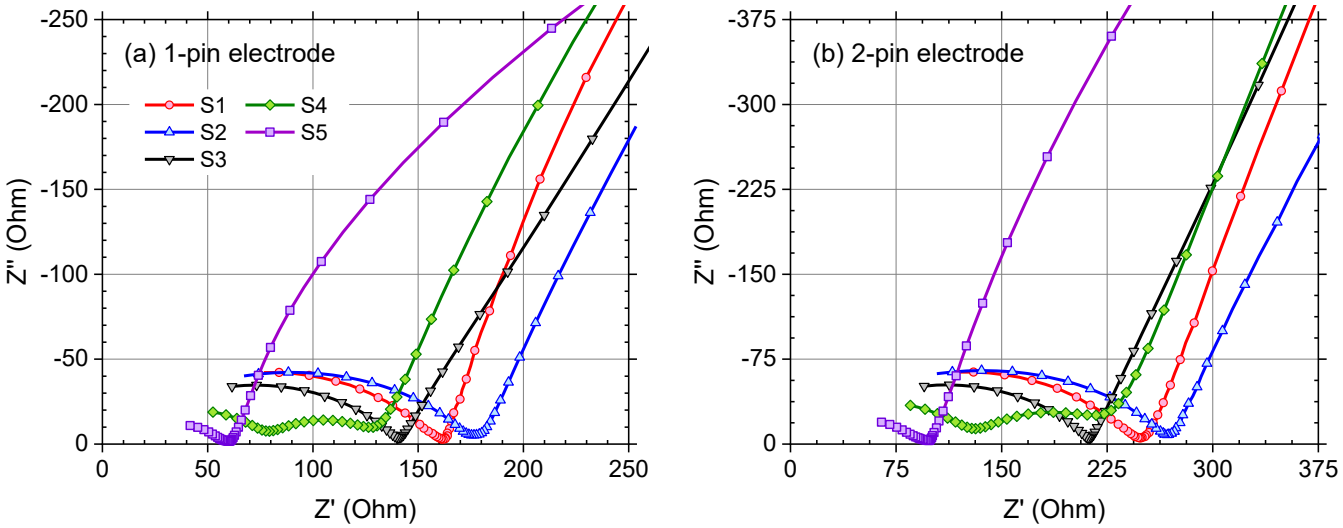

Tables 3 and 4 present key parameters identified from the Impedance response of each sealant when measured using either the coaxial electrode configuration or the parallel 2-pin electrode configuration. These include:

(i) The frequency at which Reactance is at a minimum

This location is referred to as the cusp point, effectively dividing the bulk material response on the left-had side of the response from the material/electrode interface response on the right-hand side.

(ii) The Resistance at the Cusp frequency

This parameter is generally regarded as the true bulk properties of the sealant material.

(iii) The Conductivity at the Cusp frequency

This is the reciprocal of (ii) and hence this parameter can also provide an approximation of the direct current Conductivity of the sealant material.

Table 3: Key parameters in Coax Impedance plots

Sealant	Cusp Frequency, kHz	Cusp Resistance, Ohm	Cusp Conductivity, S/m
S1a	4	167.9	0.0380
S2c	5	178.8	0.0357
S3b	10	140.7	0.0453
S4b	5, 250	126.6, 93.5	0.0504, 0.0682
S5b	10	61.3	0.1041

Table 4: Significant parameters in 2-Pin Impedance plots

Sealant	Cusp Frequency, kHz	Cusp Resistance, Ohm	Cusp Conductivity, S/m
S1b	6.3	249.0	0.0384
S2a	7.9	268.1	0.0357
S3b	10	212.4	0.0450
S4a	5, 250	190.5, 136.2	0.0502, 0.0702
S5a	10	98.2	0.0974

The Resistance observed at the cusp frequency is typically regarded as a reliable indicator of the true bulk value at zero frequency. However, in the case of Sealant S4, the dual cusp effect is evident at both relatively low and high frequencies. This raises the possibility that the true bulk Resistance may lie along the middle arc, introducing complexity into its interpretation.

Conductivity, as obtained from the impedance spectra, can be derived from impedance measurements using the following equation:

$$\sigma(\omega) = \frac{Z'(\omega)}{Z'(\omega)^2 + Z''(\omega)^2}\frac{1}{k} \qquad \text{Equation (2)}$$

where $Z'(\omega)$ is the real component of impedance (resistance) and $Z''(\omega)$ is the imaginary component of impedance (reactance).

Figure 22 illustrates the frequency-dependent conductivities of each sealant, derived from both electrode configurations. On each plot, the solid data point represents the cusp frequency, which directly corresponds to the conduction value of conductivity.

The conductivity of the sealants displays a clear variation, increasing in the order of S2 < S1 < S3 < S4 < S5, with values ranging between 0.036 S/m and 0.010 S/m, as shown in **Tables 3 and 4**. It should be noted that conductivity is influenced by pore-fluid conductivity, which can impact the bulk conductivity value. However, this variation is unlikely to differ significantly among the three OPC-based sealants. Examining the bulk conductivity values of these sealants suggests that Sealant S2 is likely to be less permeable than Sealant S1, whereas Sealant S3 is expected to be more permeable than Sealant S1.

Sealant S5, which contains chemical activators (alkali), is anticipated to have a considerably higher ionic content. This is likely to elevate its pore-solution conductivity (studies have indicated an increase of 2–3 times), resulting in a greater overall conductivity. The absence of pore-fluid conductivity data makes it challenging to accurately determine the relative permeability of Sealant S5 compared to the other sealants.

Finally, the higher conductivity of Sealant S4 suggests that it exhibits greater permeability than the OPC-based sealants.

Figure 22. Post-curing Conductivity plots of Sealants S1-S5

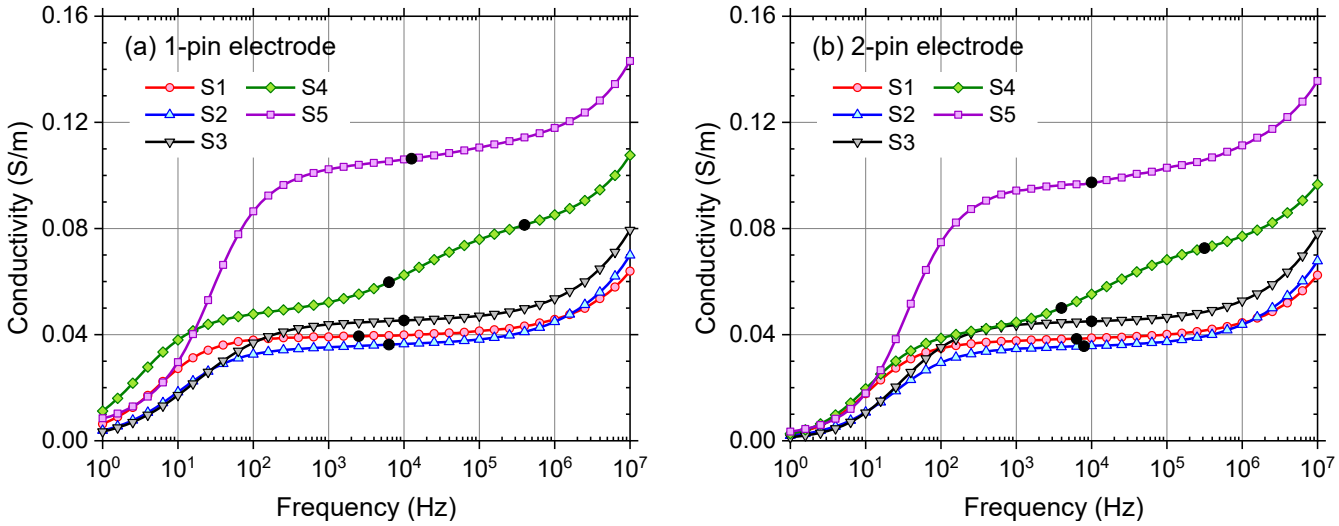

4.3.8.2 Post Exposure: Effect of Corrosion

Figures 23(a) and (b) illustrate the impedance responses measured across all LabCorr samples over the frequency range of 1 Hz to 10 MHz, with **Figure 23(a)** presenting the responses obtained 18 days after casting (prior to the application of current) and **Figure 23(b)** showing the responses recorded between 18 and 83 days. It is important to note that no nulling of lead-inductive effects has been applied across the full frequency range in these plots and that the current for the accelerated corrosion was activated from Day 26 onwards.

As illustrated in **Figure 23(a)**, all samples display a consistent response characterised by a spur at the low-frequency end of the curve (which forms part of a larger arc) and a bulk response at the high-frequency end. As note earlier, the spur is indicative of the behaviour at the sample/sealant interface, which is of particular interest. At this stage, no evidence of an additional polarising layer effect at the low-frequency end, such as due to corrosion exposure, has been observed.

With reference to **Figure 23(b)**, it is apparent that the impedance spectra for samples exposed to no accelerated corrosion (left-hand plot) exhibit a consistent shift of the spectra to the right, signifying pore densification due to ongoing hydration. No significant changes in the spur at the low-frequency end of the curve were detected. For samples subjected to a 15mA current (middle plot), a similar trend can be observed, though changes in the radius of the spur at the low-frequency side of the curve are now noticeable. These changes may indicate corrosion at the sample/sealant interface.

In samples exposed to a current of 30mA, a more pronounced shift of the spectra to the right is evident. This suggests that prolonged exposure to current influences not only the sample/sealant interface but also accelerates the cement hydration process. This acceleration could potentially explain the previously noted increase in apparent bond strength, as seen in **Figure 13**.

Figure 23. Impedance response for (a) Day 18 and (b) Days 18 – 83 (no nulling).

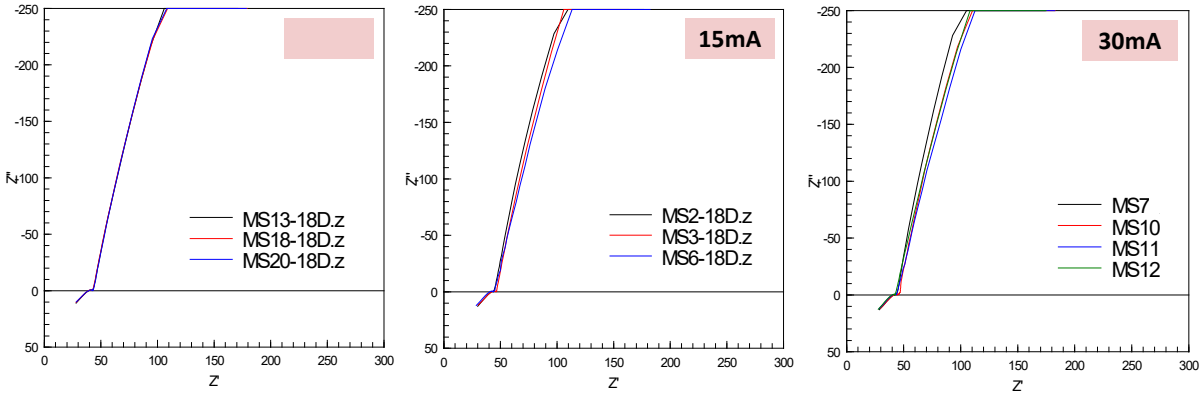

(a)

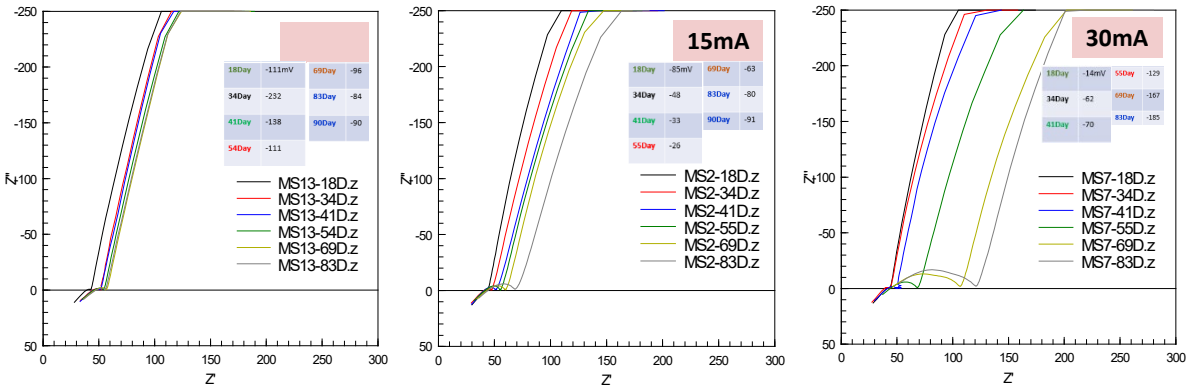

(b)

Figure 24 illustrates the impedance responses for all samples tested on Day 83. It is evident that extended exposure to corrosion has had a significant impact on the overall behaviour. In particular, the samples exposed to the higher current of 30mA exhibit a much greater variation in their impedance spectra compared to those subjected to lower currents or no current at all. This increased variation is likely due to the inherently complex nature of corrosion processes. Following post-testing sample extraction, it was observed that corrosion progressed unevenly, resulting in more pronounced differences in both the extent and distribution of corrosion across the samples (refer to **Figure 13**).

Figure 24. Impedance response (no nulling) for (a) Day 18 and (b) Days 18–83.

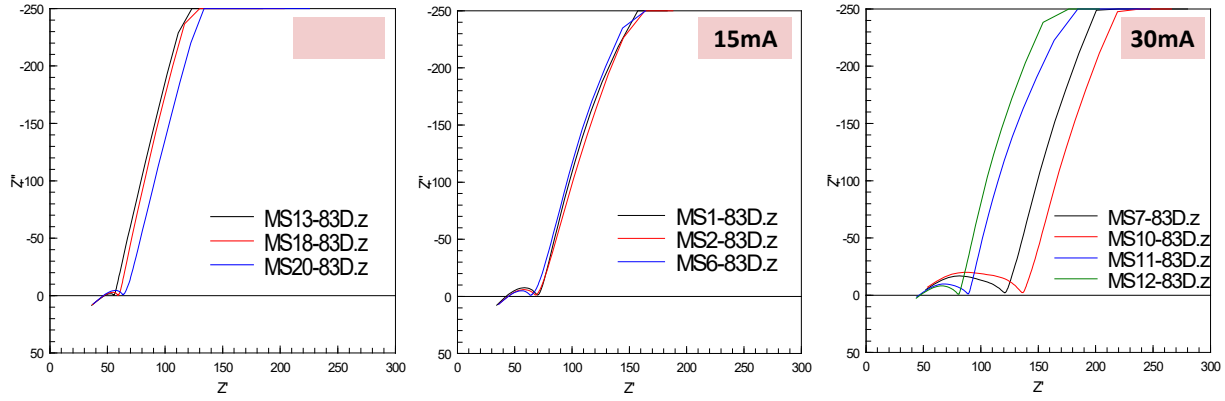

To gain deeper insights into the effects of prolonged exposure to corrosion, **Figure 25(a)** illustrates the responses of three individual samples subjected to current levels of 0mA, 15mA, and 30mA over the entire exposure period. A summary of the bulk resistance for these representative samples is shown in **Figure 25(b)**. As noted earlier, the applied current levels correspond to current densities of 0, 0.21, and 0.42 mA/cm², respectively. The results indicate that the samples exhibited distinct responses depending on the current level applied. The low-frequency region of the curve, which forms part of a larger arc, primarily reflects the behaviour at the sample/sealant interface and is of particular interest. All samples demonstrated a gradual shift to the right-hand side of the curve, which can be attributed to the self-curing process of the sealant. For samples exposed to prolonged electrical currents, this shift was significantly more pronounced, likely due to additional curing effects induced by the application of electrical current required to facilitate the corrosion process.

Broadly, three distinct stages of response were observed:

(i) An initial phase with increasing resistance due to curing.

(ii) A transitional phase where resistance increased further, likely resulting from a combination of additional curing effects and corrosion at the steel casing/sealant interface.

(iii) A final phase where resistance continued to rise, predominantly driven by further curing effects and likely corrosion at the interface.

The observed increase in bulk resistance suggests that the application of electrical current enhanced cement hydration, which may have partially contributed to the previously reported increase in apparent bond strength, as shown in Figure 13.

Figure 25. Impedance response (no nulling) for (a) Day 18 and (b) Days 18–83

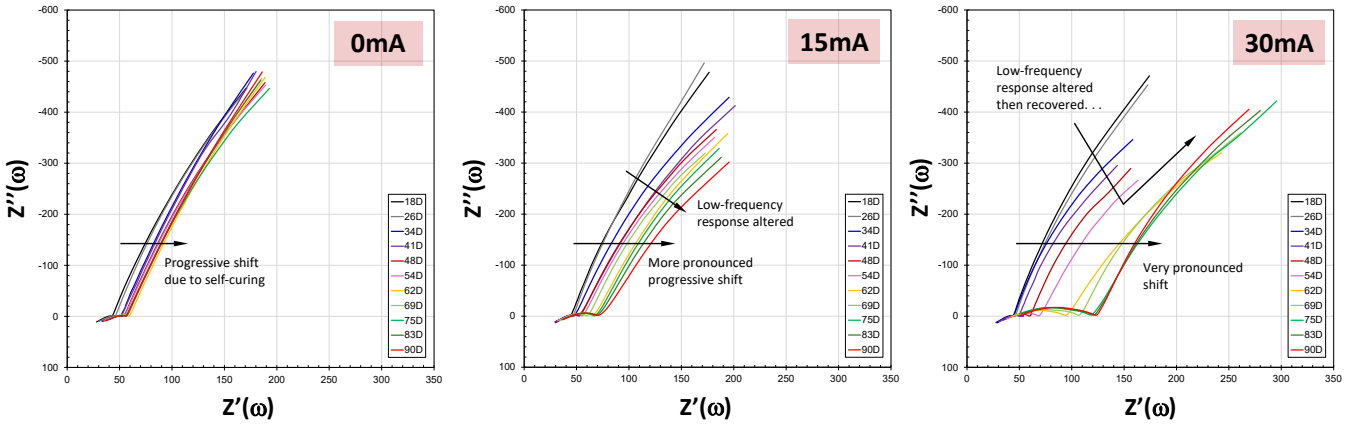

(a)

Figure 25. Impedance response (no nulling) for (a) Day 18 and (b) Days 18–83 (continued)

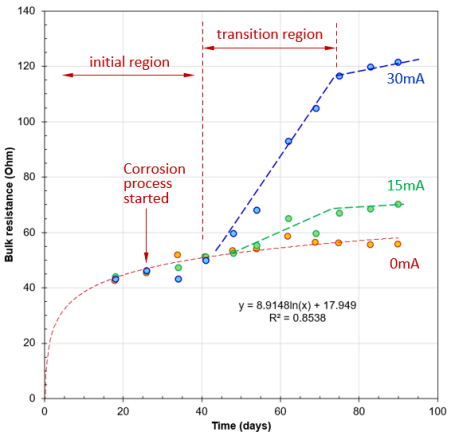

(b)

In addition to influencing the resistive component, corrosion at the steel casing/sealant interface is anticipated to introduce capacitive effects to the overall system. This is attributed to the development of corrosion products at the sealant/steel interface, which possess distinct properties that can alter the electrical characteristics of the system. To investigate this phenomenon, electrical circuit analysis was performed by modelling the low-frequency portion of the impedance spectra using an equivalent circuit comprising a resistor and capacitor connected in parallel. The low-frequency range was deliberately selected, as this region effectively captures the behaviour at the sealant/steel casing interface, where the effect of corrosion is expected to be the most prominent.

An example of the circuit parameters obtained from this analysis is shown in **Figure 26**. As can be seen, both the resistive and capacitive components of the equivalent circuit were influenced by the prolonged induced corrosion, indicating that corrosion at the sealant/casing interface not only alters the interface characteristics but also impacts the overall response.

Figure 26. Equivalent circuit modelling on the low-frequency response

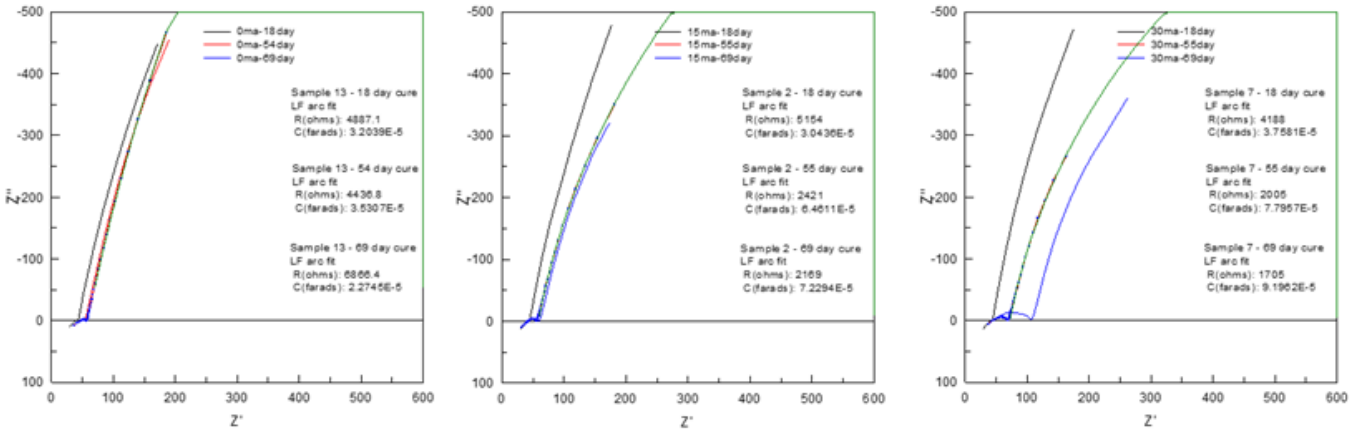

Figure 27 displays the impedance response of autoclave-cured Sealant S1-S5 samples subjected to both high-temperature curing and corrosion regimes. Based on earlier measurements, the current was initially set at 30mA. However, after 2 days, this was further reduced to 20mA and subsequently switched off after 7 days, as the voltage in several samples approached the upper limit of the power supply. This would suggest that high-temperature exposure significantly increased the likelihood of corrosion initiation, with the rapid increase in voltages suggesting that corrosion progresses more rapidly at the sealant/casing interface than the lab-cured samples. The current application was then resumed at 5mA starting from Day 14. From **Figure 27**, it is interesting to note that all sealants produce a significantly different impedance response at the beginning of testing (Day 0). The impedance spectra of the sealants at Day 14, post initial corrosion regime, are comparable to those measured at the start of experiment (prior to current application), particularly on the shape and extent of the high-frequency bulk arc. This would indicate that there was virtually no additional curing and could be associated with the fact that this series of samples was subjected to the enhanced curing regime (elevated temperature and pressure). It is however interesting to note that the spur at the low-frequency end showed notable changes, which is generally much shorter.

Figure 27. Impedance response of Sealants S1-S5 before and after exposure

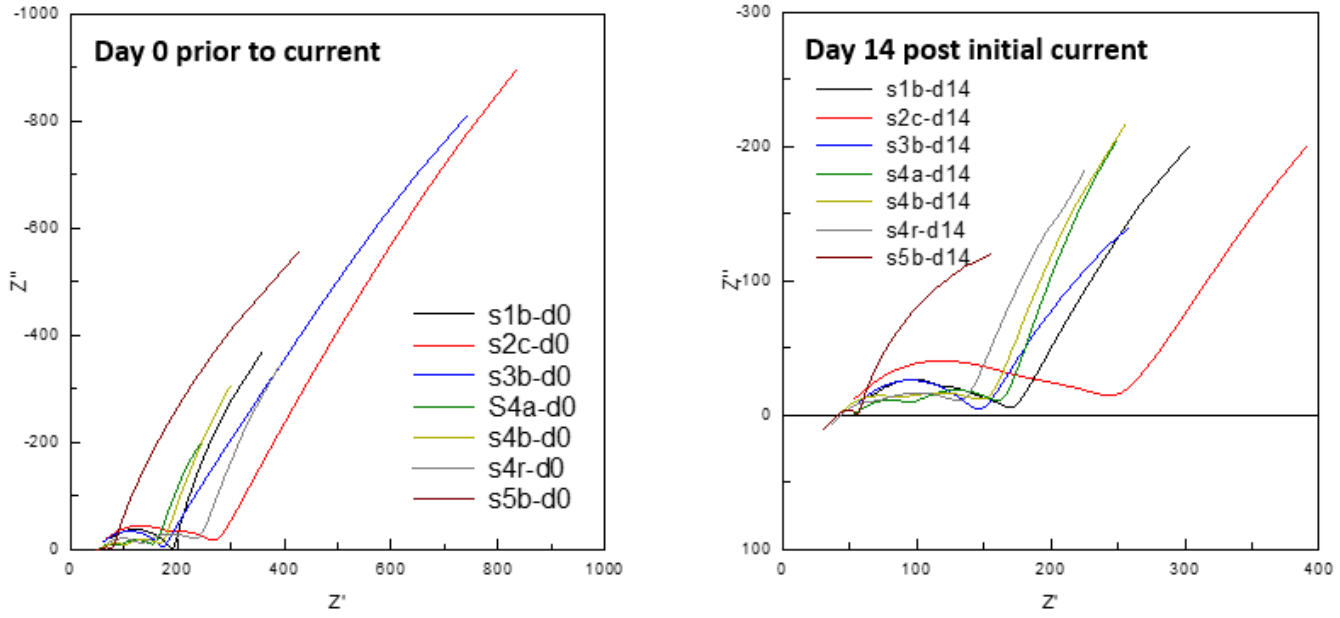

4.3.8.3 Effect of Temperature

The impedance measurements discussed earlier were undertaken at a controlled laboratory temperature of 20°C and under ambient pressure. In order to provide insights into the influence of temperature and pressure on the relative bulk permeation properties of the sealants, samples of Sealants S1 to S5 (including Sealant S4R) were fabricated and exposed to varying temperatures ranging from 20°C and 150°C range under a pressure of 300 bars. These samples were initially subject to 150°C for a period of up to 31 days, after which the temperature was gradually reduced to 20°C in 7 days, at a rate of approximately 0.77°C per hour. During this temperature changes, the Resistance of the samples were continuously monitored using a bespoke data logger, which recorded 2 measurement data per hour.

Figures 28(a) and (b) present the measured resistance over a 7-day period, with (a) displaying the complete dataset for the five sealants and (b) providing a magnified view for the four sealants. It is evident that the bulk Resistance of all the sealants increases significantly, displaying a highly nonlinear response as the temperature decreases from 150°C to 20°C. Due to the elevated curing, the cement hydration and other associated reactions can be assumed to have effectively ceased, and that the ionic concentration within the pore fluid to also have stabilised. Hence, the marked rise in resistance can be attributed solely to the effects of temperature. These effects arise from the reduced mobility of ions within the pore structure of the sealant body, as the temperature decreases, thereby causing the overall increase in bulk Resistance.

To gain a clearer understanding of the temperature effect, this temperature-dependent behaviour is represented in the Arrhenius format, viz,

$$R = R_{\mathrm{o}}\, e^{\left(\frac{E_{\mathrm{a}}}{R_{\mathrm{g}}T}\right)} \qquad \text{Equation (3)}$$

where R (Ohm) is the electrical resistance of the sealant measured at temperature T (Kelvin); R_{o} is a pre-exponential factor, representing the nominal value at infinite temperature; E_{a} is the activation energy for ionic conduction in cement matrix (J/mol), R_{g} is the Universal Gas constant (8.31446 J/(mol.K)). Equation (3) can be converted into a simple linear form by applying the natural logarithm to both sides, resulting in

$$\ln R = \frac{E_{\mathrm{a}}}{R_{\mathrm{g}}}\left(\frac{1}{T}\right) + \ln R_{\mathrm{o}} \qquad \text{Eq. (4)}$$

Figure 28. Resistance of Sealants S1-S5 measured over a temperature range of 20-150°C

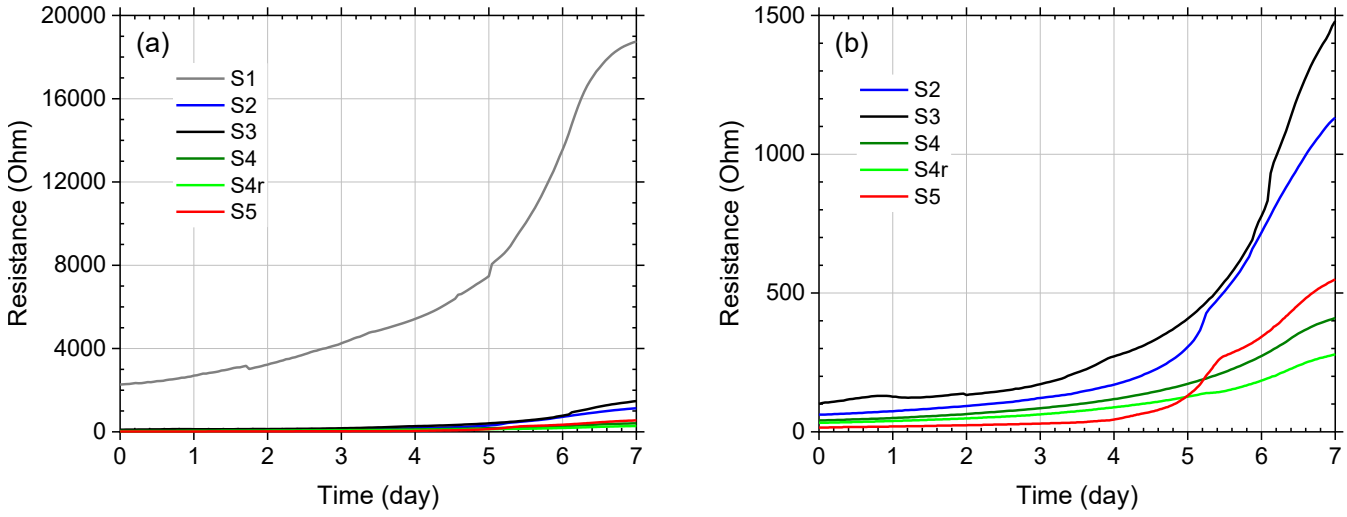

Figure 29 (a) presents the plots of the natural logarithm of bulk Resistance (Ln R) for each sealant plotted as a function of 1000/T. It is interesting to note that the highly nonlinear curves observed earlier have transitioned into less nonlinear response, with a linear relationship emerging over certain temperature ranges. Interestingly, Sealants S4 and S4R display a predominantly linear response across the entire temperature range 150°C → 20°C. Building upon the linearity of Equation (3), determining the slope of each curve over a certain

temperature range can provide useful information. The slope can subsequently be multiplied by R_g to calculate the activation energy, expressed in kJ/mol. The activation energy, in this context, can be interpreted as the energy barrier that ions must overcome to enable conduction within the pore network. Hence this parameter can offer insights into the pore connectivity of the individual sealants. A constant activation energy across a certain temperature range would indicate that ionic conduction through the pore network is the prevailing mechanism, with no physical alterations in the connectivity of the pore structure. To this end, the activation energy was evaluated between 80°C and 120°C, corresponding to the typical operational temperature of a well. Figure 29 (b) provides an example for Sealant S2, with the data point fitted using a linear equation. The activation energy values recorded for all sealants within this temperature range were largely comparable: 16.73 kJ/mol, 17.13 kJ/mol, 17.03 kJ/mol, 17.39 kJ/mol, and 14.30 kJ/mol for Sealants S1 through S5, respectively. Sealant S5 displayed a notably lower value, which could be attributed to its higher ionic content. Notably, there are specific temperature ranges below 80°C where an increase in slope is evident as temperature decreases. Although this temperature range currently falls outside the primary area of interest at present, this approach could be further explored to assess how pore connectivity for a particular sealant changes with variations in temperature.

Figure 29. Arrhenius plots for (a) Sealants S1-S5 over the temperature range 20-150°C and (b) Sealant S2 over the temperature range 80-120°C.

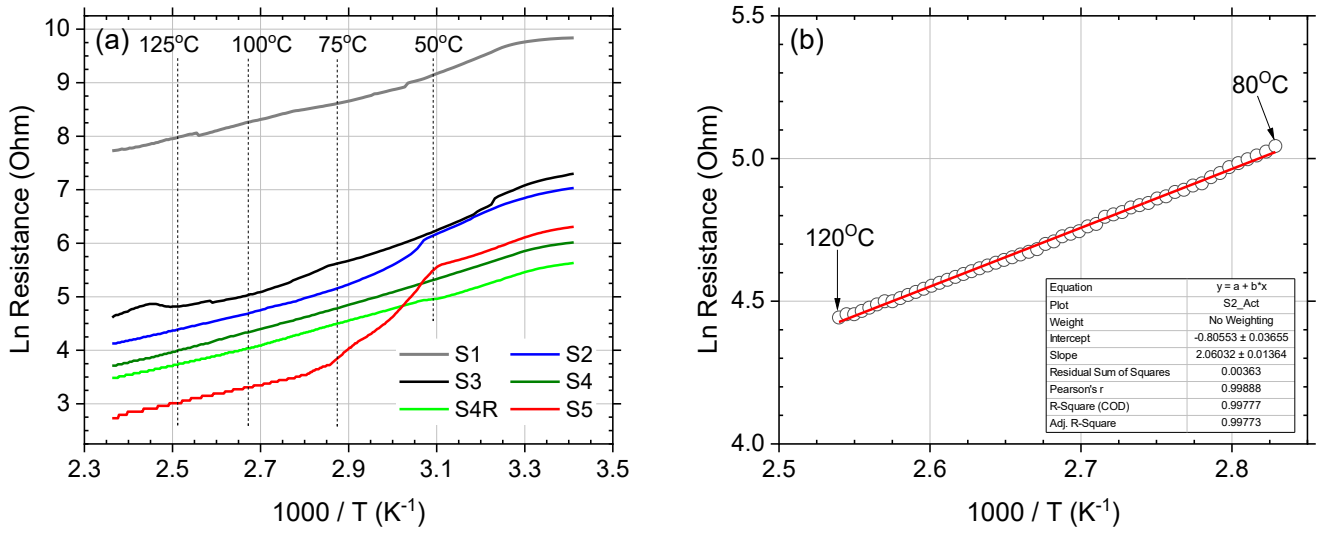

4.3.9 Comparison between Properties

In this section, the data obtained from both the shear-bond testing and electrical measurements are compared. The parameters of interest include the compressive strength of the sealants, shear bond strength, and characteristics related to bulk resistance and capacitance. Furthermore, permeability is also taken into account in this analysis, as it offers an interesting comparison with the bulk resistance values obtained from the different sealants, which represent the connected porosity of the sealants, as previously discussed.

Figures 30(a) and (b) illustrate the observed relationships between the evaluated parameters between the mechanical properties obtained from shear-bond testing and electrical measurements. With reference to **Figure 30(a)**, there appears to be a notable correlation

between bulk resistance and compressive strength, which is somewhat unexpected. Bulk resistance typically indicates the level of connected porosity within the sealant, while compressive strength is indicative of the overall structural integrity of the pore network. The apparent correlation between these parameters is interesting and warrants further investigation. In contrast, as shown in **Figure 30(b)**, the comparison between bulk resistance and mean bond strength reveals only a weak correlation. It is important to highlight that Sealant S4 experienced premature failure, which could have skewed the perceived trend. When the analysis is restricted to Sealants S1 to S3, the relationship between bulk resistance and mean bond strength seems to flatten, presenting a horizontal trend. This would indicate that there is little to no correlation between these two parameters. The lack of correlation can be attributed to the different characteristics these parameters represent. Bulk resistance measures the overall bulk properties of the material, such as its porosity and connected pathways. On the other hand, mean bond strength is primarily determined by the interfacial properties at the sealant/casing interface. This distinction emphasises that the mean bond strength cannot be estimated from the bulk resistance.

Figure 30. Comparisons of bulk resistance with measured compressive and mean bond strengths.

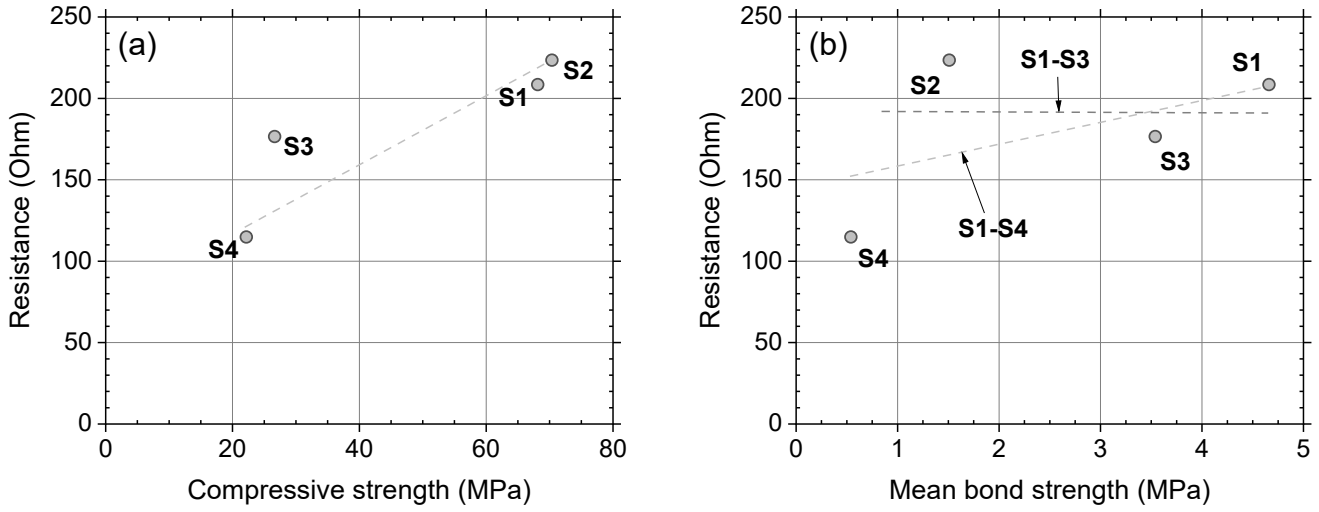

The correlation between the parameters obtained from the equivalent circuit modelling and mean bond strength is presented in **Figures 31(a) and (b)** for samples subjected to no current, 15mA, and 30mA (current densities of 0, 0.21, and 0.42 mA/cm2, respectively). Overall, it was found that the application of the electrical current not only facilitates corrosion at the sealant/sample interface but also influences the hydration and curing processes.

As can be seen from **Figure 31(a)** that there is a strong correlation between bulk resistance and the mean bond strength, and this could be attributed to the additional curing effects caused by the application of electrical current, which is required to drive the corrosion process discussed above. Interestingly, the data also show a substantial increase in the capacitive component when correlated with the mean bond strength across the various samples. This observation suggests that the capacitive behaviour may serve as a valuable indicator for monitoring the likelihood of corrosion initiation at the sealant/casing interface.

The capacitive component, reflective of the changes occurring at the interface, provides further insight into the effects of corrosion and could have broader implications for detecting corrosion initiation at the sealant/casing interface.

Figure 31. Comparisons of bulk electrical properties and mean bond strength after exposure

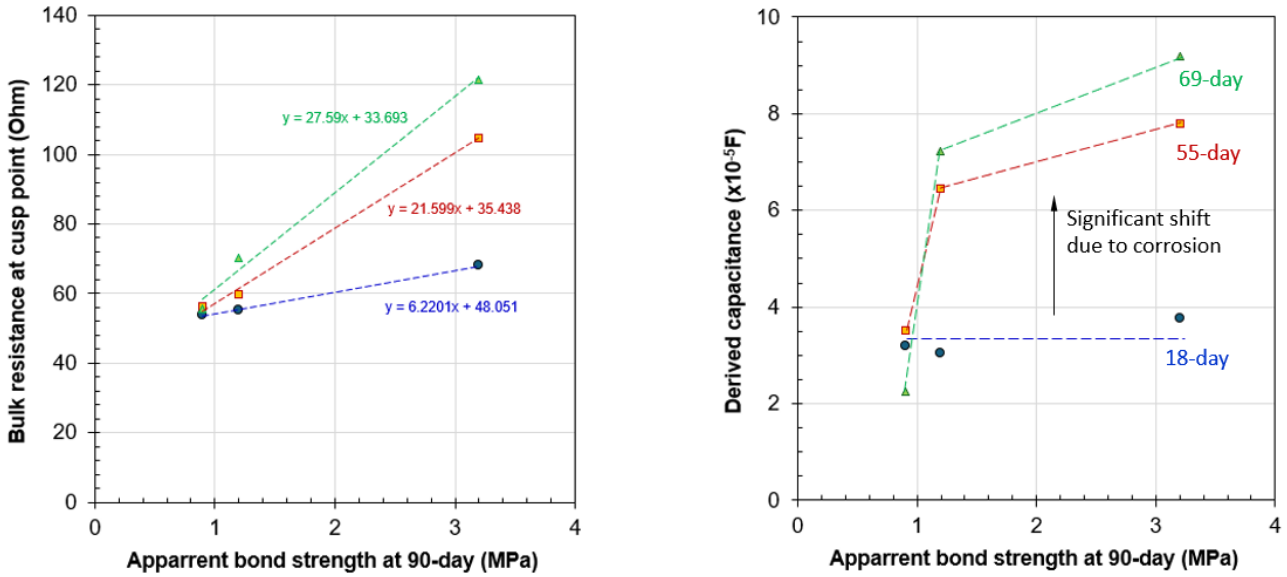

With regards to the bulk electrical properties, **Figure 32** illustrates the conductance (the reciprocal of bulk resistance) calculated from the impedance data, plotted against the water permeability measurements of unexposed reference samples reported by our project partner in WP 1. For the three PC-based sealants (Sealants S1–S3), it can be assumed that the pore fluid compositions are broadly similar to allow for a direct comparison. In contrast, for Sealant S5, the pore fluid is expected to exhibit a significantly higher ionic strength due to the activators incorporated into this material (a value of two to three times has been reported in previous studies). For Sealant S4, the pore fluid composition may also differ. Additionally, Sealant S4 has a more complex frequency-dependent behaviour which makes it more difficult to determine an accurate conductivity based on the available data. Overall, **Figure 32** displays that there is a somewhat correlation between conductance and permeability, with the conductivity increasing with increasing permeability as one would expect. Interestingly, Sealant S4 demonstrates relatively low conductance in relation to its permeability, potentially due to a lower ionic strength in the pore fluid. Conversely, Sealant S5 exhibits comparatively high conductivity relative to its permeability, which may indicate that its pore-fluid conductivity might be much higher than that of the PC-based materials (i.e., Sealants S1–S3). From the spread of the data, it appears that the pore fluid conductivity in this sealant is approximately twice that of the PC-based sealants, which broadly aligns with findings reported in published literature. The findings presented suggest that electrical measurements could offer a means of evaluating seal permeability, provided those factors influencing electrical impedance, such as pore fluid composition, are properly accounted for.

Figure 32. Comparisons of bulk conductance and material permeability

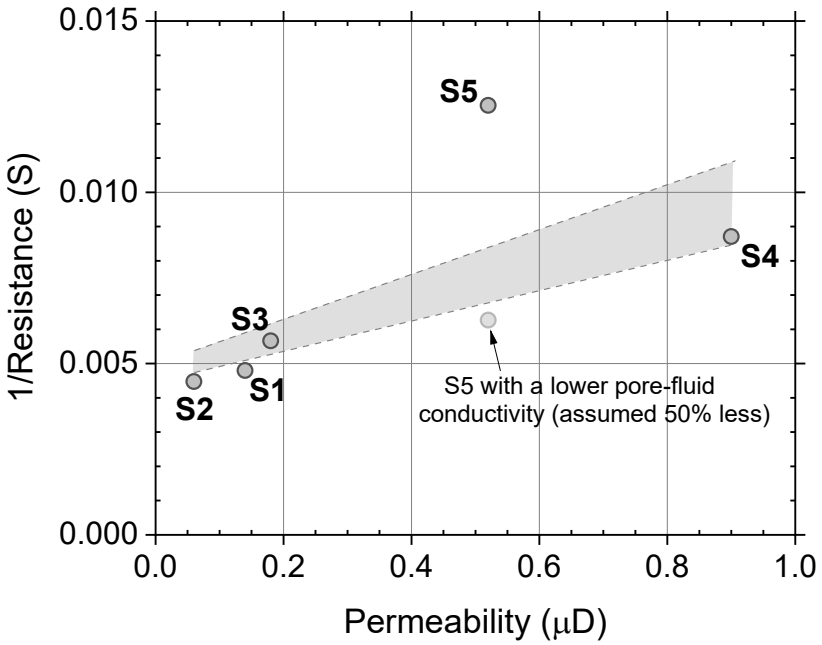

4.4 Concluding Remarks

Laboratory investigations involving shear bond tests and electrical measurements were undertaken to evaluate the performance of five distinct sealants encased within cylindrical steel casing. Samples were cured under two conditions: standard laboratory conditions at approximately 20^{o}C and elevated temperature (up to 150^{o}C) and pressure (300 bar) to replicate the conditions typical of deep offshore CCS wells. Key observations:

(1) Sample Holder Design. A specialised sample holder was created to replicate a miniature plugged well-bore. The robust design incorporates a steel casing, PTFE caps, and a new electrode arrangement, tailored for enhanced curing conditions up to 150°C and pressures of up to 300 bar. This design successfully eliminated radial cracking observed in original design.

(2) Electrical Monitoring during Curing. Electrical monitoring during enhanced curing facilitated the observations of the intricate hydration and hardening processes of the five sealants. Maintaining 150°C for three weeks was generally sufficient to ensure near-complete hydration, achieve stable properties, and maximise the performance of all sealant materials tested.

(3) Shear Bond Strength. Bond strengths exhibited significant variability across sealants, ranging from 0.54 MPa for Sealant S4 to 4.66 MPa for Sealant S1 samples. Factors such as curing conditions, sealant setting time, and corrosion at the sealant/casing interface played a dominant role. Compressive strength influenced bond strength, but it did not guarantee good bonding performance, as evidenced by the result obtained from Sealant S2 samples.

(4) Sealant Performance. Of the five sealants tested, Sealant S3 displayed superior bond strength despite moderate compressive properties, while Sealant S1 displayed elevated bond

strength attributed to corrosion at the interface. Sealant S4 experienced premature failure likely due to rapid setting, which was mitigated by the use of retarding agents, significantly enhancing bond strength. Sealants S1R and S5 demonstrated markedly improved bond strengths, with Sealant S5 achieving the smoothest de-bonded interface and minimal evidence of corrosion. The reasons for this significant increase were not clear and could potentially involve a few factors such as errors in the preparatory stage or during material batching.

(5) Impact of Curing Conditions. Elevated curing temperatures and pressures improved both shear bond and compressive strengths. High pressure minimised volumetric changes, enhancing bond properties. Extending setting times during the initial increase in temperature also proved beneficial, particularly for rapid-setting sealants like Sealant S4. The adjustment of setting times could also be applied to other sealants to improve their bonding efficacy with metal casings.

(6) Corrosion and Bond Strength. Corrosion levels varied among the test sealants, being most pronounced in Sealant S1 samples. Sealants S3 and S5 exhibited the lowest corrosion levels, while Sealant S4 exhibited moderate levels in both the initial and repeated tests, with higher bond strength observed in the latter. Accelerated corrosion affected the sealant/casing interface, artificially increasing bond strength. However, this enhancement is expected to diminish over time due to creep and shrinkage within the sealant body. Consequently, bond strength measured in the presence of corrosion should not be considered a reliable performance indicator.

(7) Electrical Measurements Post Curing: Electrical conductance trends correlated with sealant permeability, suggesting that conductivity measurements can offer valuable insights into sealant permeability, provided factors like pore solution conductivity are accounted for. Low-frequency impedance responses, particularly the capacitive component, may serve as indicators for detecting the initiation and extent of corrosion.

4.5 Key Project Outcomes

Bond properties before exposure and electrical testing at initial stage

Sealant Bond Performance. Testing highlighted variations in bond strength and stiffness, with mean bond strengths decreasing in the order S1 > S3 > S2 > S4. Physical examinations revealed contrasting corrosion levels, with S1 showing extensive corrosion and S2 and S3 displaying minimal or no corrosion. The regulation of setting times curing significantly improved bond strength, as evidenced by repeated tests with Sealant S4. Final tests with sealants S1 (repeat) and S5 achieved much higher mean bond strengths. The reasons for these elevated strengths were unclear, but it was confirmed that Sealant S5 had the smoothest interface with metal casing with no evidence of corrosion.

Electrical Measurement during Enhanced Curing. The methodology presented is shown to effectively monitor the intricate hydration and hardening processes of all sealants tested. A temperature of 150°C sustained for three weeks was generally sufficient to ensure near-

complete hydration, achieve stable properties, and maximise the performance of all sealant materials across the board.

Bond properties after exposure and electrical testing

Post-Exposure Bond Properties. Accelerated corrosion influenced the curing process, resulting in artificial bond strength enhancements, particularly in sealants with high modulus elasticity. Nonetheless, these improvements are temporary and likely to reduce over time due to the creep and shrinkage of the sealant body. Consequently, bond strength observed under corrosive conditions should not be used as a performance indicator. Moreover, the combined effects of corrosion expansion and sealant deformation may increase porosity at the interface as corrosion progresses, potentially creating leakage pathways. The use of non-corrosive casing and/or sealants designed to minimise the likelihood of corrosion initiation is considered essential.

Electrical Measurements Post Enhanced Curing. Variations in sealant conductivity were observed, increasing in the sequence S2 < S1 < S3 < S4 < S5, with values ranging from 0.036 S/m to 0.010 S/m.

Comparative Assessment between Properties

Shear bond properties. Sealants S2 and S4 displayed bond strengths within the reported ranges when compared with previously published data, whereas Sealants S1 and S3 generally displayed higher bond strength values. A similar trend was observed for Sealants S1 repeat and S5. Compressive strength influenced bond strength, but it did not guarantee good bonding performance, as evidenced by the result obtained from Sealant S2 samples. Apparent stiffness, derived from shear bond testing, provided additional insights into bonding performance and was found to correlate with the modulus of elasticity of the sealants. The conditions at the sealant/casing interface were found to influence the apparent bond strength and stiffness of the sealant samples with metal casing.

Mechanical and electrical properties. No significant relationship was observed between bulk resistance and mean bond strength, as these parameters represent distinct material properties. A correlation between bulk resistance and compressive strength was observed which warrants further investigation.

The application of electrical current was found to influence both corrosion at the sealant/casing interface and the curing process, with bulk resistance showing a strong correlation with mean bond strength under these conditions. A significant increase in capacitance was observed, suggesting its potential as an indicator for monitoring corrosion initiation at the sealant/casing interface. For the sealants tested in this project, a general trend of increased conductivity with higher permeability was observed, indicating the potential of electrical measurements in evaluating sealant permeability, provided pore fluid composition is adequately considered.

Effect of key parameters

The shear bond strengths were found to be influenced by a range of factors, with curing conditions, sealant setting time, and corrosion at the interface between the sealant and steel casing emerged as the dominant factors. Key findings indicate that higher curing temperatures and pressures significantly enhanced both shear-bond strength and compressive strength. Elevated pressure, in particular, effectively reduced volumetric changes, leading to enhancements in bond strength.

Regarding corrosion at the interface, while this was found to increase mean bond strength, this effect is considered non-permanent and likely to reduce over time due to creep and shrinkage in the sealant matrix. As such, the mean bond strength in the presence corrosion is not a reliable indicator of performance.

Extending the initial setting period, such as controlling the rapid setting of Sealant S4 during initial temperature increases, proved beneficial. This adjustment is particularly relevant during well plugging, where temperatures typically increase with depth, following the thermal conditions of the surrounding rock formations, which for offshore reservoirs at depths of 2 to 3 km, generally ranging between 80^{o}C and 120^{o}C. The regulation of setting time could be applied to other sealants to improve their bonding with surrounding casing.

5.0 Financial Summary

This work presented in this report was undertaken between October 2021 and December 2024, with funding of £274,477.76 provided, covering 80% of the full economic costs.

6.0 Dissemination Activities

Throughout the project, Heriot-Watt University engaged in the following dissemination activities:

Presentations

Open seminar: Van Noort, R., X. Qiu, K. Li and G. Starrs (2023) Ceminar #1. Open CEMENTEGRITY Webinar, 2023-03-16.

Open seminar: Van Noort, R., K. Li, G. Starrs, H. Hajiabadi and M. Gupta (2024) Ceminar #3. Open CEMENTEGRITY Webinar, 2024-06-06.

Open seminar: Van Noort, R., H. Hajiabadi, M. Gupta, G. Lende, A. Pluymakers, B. Suryanto and A. Kvassnes (2024) Concluding Ceminar (#4). Open CEMENTEGRITY Webinar, 2024-11-27.

Open seminar: Van Noort, R., K. Li, B. Suryanto (2024) Enhancing Sealant Durability and Integrity During CCS – The CEMENTEGRITY Project. Webinar for SPE, 2024-11-14.

Presentation to regulator: Van Noort, R., Lende, K., Pluymakers, A., Starrs, G. (2024) Cementegrity Webinar for Regulators, 2024-12-10.

Articles

Van Noort, R., M. Gupta, S. H. Hajiabadi, M. Khalifeh, A. Kvassnes, K. Li, A. Pluymakers, G. Starrs, B. Suryanto, G. Svenningsen, G. Ye (2024) Development and testing of novel cement designs for enhanced CCS well integrity. 17th Greenhouse Gas Control Technologies Conference 2024 (GHGT-17) proceedings, https://ssrn.com/abstract=5010396.

Van Noort, R., A. Pluymakers, K. Li, B. Suryanto, G. Starrs (2024) Development of tailored wellbore sealants for CCS and other geological storage applications. First Break 42, p. 89-94.

Van Noort, R., B. Suryanto, G. Starrs, G. Lende (2023) Testing and developing improved wellbore sealants for CCS applications. 12th Trondheim Carbon Capture and Storage Conference (TCCS), 06/19-06/21, Trondheim, Norway.

Van Noort, R., M. Gupta, S. H. Hajiabadi, M. Khalifeh, A. Kvassnes, K. Li, A. Pluymakers, G. Starrs, B. Suryanto, G. Svenningsen, G. Ye (2024) Development and testing of novel cement designs for enhanced CCS well integrity. GHGT-17 2024, 10/20-10/24, Calgary, Canada.

Suryanto, B., G. Starrs, A.J.S. Kvassnes (2024) Assessment of Bond Strength of Various Cementitious Sealants for CCS Well Applications. Joseph Aspdin 200 International Symposium, 2024-07-12, Edinburgh, UK.

Starrs, G., B. Suryanto (2024) The electrical properties of cementitious sealants for subsea CCS applications. Joseph Aspdin 200 International Symposium, 2024-07-12, Edinburgh, UK.

Reports

Suryanto, B. & G. Starrs (2025) Characterisation and monitoring of oil-well cements under simulated CCS well conditions. CEMENTEGRITY Deliverables 5-1 to 5-6.

7.0 Lessons Learnt and Barriers

One key lesson learnt from the project was the challenge at the beginning to establish suitable curing and exposure conditions that accurately simulate subterranean environments and appropriate for CCS applications. Initially, this process involved considerable trial and error, as

the initial design proved ineffective. We received a lot of support from Halliburton Norway, whose contribution was invaluable to develop protocols for high-temperature and high-pressure curing. They also provided access to their state-of-the-art laboratory for sample fabrication and testing, which were instrumental in resolving this issue.

Another notable challenge was the fabrication of the sealant samples. Since the sealants were proprietary blends, they had to be produced in-house at Halliburton's Stavanger facility. Despite efforts to streamline testing procedures, the process remained complex, requiring sample holders to be machined in the UK, transported to Norway, and assembled with active involvement from staff, as the sample casings were integral to the tests. The unwavering support from Halliburton Norway and the close collaboration throughout proved vital in overcoming this barrier.

A significant lesson from the project was the importance of collaboration within the consortium. The leadership and guidance provided by IFE in Norway, particularly in managing work and dissemination activities, along with the contributions of ReStone AS, were pivotal in advancing the research. Regular communication and engagement among consortium partners enabled effective comparison of methodologies and results across various work packages, helping to identify critical parameters and refine processes. Sharing of data and expertise was a crucial factor, as each consortium member brought unique knowledge and specialised facilities, benefiting the overall project. This cooperative spirit was reflected in joint publications and dissemination efforts conducted as part of the CEMENTEGRITY project.

To ensure progress was consistently monitored and shared, the project established regular online meetings, called 'Ceminars'. These open meetings provided updates from all work packages, alongside in-depth presentations by selected partners on their activities and findings. Such exchanges often led to direct collaborations, showcasing how open communication and teamwork played an essential role in overcoming barriers and enhancing the project's outcomes.

8. Project Impact

This project provides a detailed evaluation of the comparative performance of four cementitious and one non-cementitious sealant. These include two widely used in current field applications, two newly developed proprietary blends specifically designed for CCS well-plug applications, and a reference material used in existing oil and gas wells. While none of the five blends demonstrated superior performance across all aspects tested, the best outcomes may be achieved by tailoring specific blends to different sections of the wellbore, based on anticipated local conditions. Moreover, insights gained from the CEMENTEGRITY project offer opportunities to develop more versatile and well-rounded blends to address broader operational needs.

Within the wider scope of the project, WP5 contributed to the development of relatively simple test methodologies for assessing shear bond strengths. These methods allow for the evaluation of new developed sealants using facilities typically available in standard cement testing laboratories around the world. In addition, WP5 contributes to the development of non-invasive testing methodologies, with the potential for further refinement and application, not only in controlled laboratory settings but also for real-time in-situ monitoring of wellbore plugging under service conditions. The simplicity of these methodologies offers promising possibilities for application in CCS wells with operational lifespans extending beyond those of current wells.

Industry engagement played a vital role in maximising the impact of the project, promoting collaboration and ensuring the practical application of findings. Moving forward, continued efforts will prioritise the transfer of knowledge and the extension of project outcomes to support broader industrial practices. Additional funding will be sought to build on the insights gained from this study, advance test methodologies, and strengthen partnerships with industry stakeholders and academic institutions. This will help ensure sustained progress in CCS technology development while facilitating the practical application and deployment of the technology.

If you need a version of this document in a more accessible format, please email alt.formats@energysecurity.gov.uk. Please tell us what format you need. It will help us if you say what assistive technology you use.